

Contents lists available at ScienceDirect

# Chemical Geology

journal homepage: www.elsevier.com/locate/chemgeo



Invited research article



# First-row transition elements in pyroxenites and peridotites: A promising tool for constraining mantle source mineralogy

Otto I. Lang, Sarah Lambart

The University of Utah, Department of Geology and Geophysics, MagMaX Laboratory, USA

#### ARTICLE INFO

Editor: S Aulbach

Keywords: FRTEs Exchange coefficients Peridotites Pyroxenites Iceland Samoa

#### ABSTRACT

Mantle heterogeneity has a first-order control on the petrological and geochemical differences of erupted mafic lavas worldwide. Because of their contrasted distributions between mantle phases, First Row Transition Elements (FRTEs) have been considered potential lithological tracers. Using a combination of published data on natural and experimental samples and new high-precision analyses on a variety of pyroxenite samples, we investigate the parameters that control FRTE partition (Ds) and exchange (Kps) coefficients between common mantle minerals. We demonstrate that mineral-clinopyroxene exchange coefficients are independent of composition and temperature and that coefficients obtained from natural samples can be accurate as long a sufficiently high number of compositionally diverse samples are considered, making them reliable input parameters in mantle melting models. As a proof of concept, we use the exchange coefficients determined from natural mantle lithologies in this study, along with published experimental clinopyroxene/melt partitioning coefficients, to perform simple inverse modeling on two basalt suites from the Western Volcanic Zone in Iceland and Samoa, selected for their contrasted Mn/Fe and Zn/Fe ratios. Our results show that a given FRTE ratio in basalt can be explained by a large range of modal proportions in the source. However, when combined, FRTE ratios become a powerful tool to constrain the nature of the source.

# 1. Introduction

It is now collectively believed that the asthenospheric mantle is heterogeneous chemically. For example, the isotopic composition, the trace element concentrations, and, to a lesser extent, the major element composition vary. However, arguments continue on the necessity to involve lithological variability (i.e, peridotites and pyroxenites present in the mantle as distinct bodies) to accommodate this chemical variability. The conclusion of lithological differences in the mantle arises mainly from the failure to produce the range of compositions for Mid-Ocean-Ridge Basalts (MORBs) and Oceanic Island Basalts (OIBs) found from melting peridotite alone, which has led many to suggest that a separate pyroxene-rich source lithology may be present throughout melt generating zones in the mantle (e.g., Elkins et al., 2019; Hirschmann and Stolper, 1996; Hofmann, 1997; Kogiso et al., 2004;; Lambart et al., 2016, 2019; Mallik et al., 2021; Sobolev et al., 2007; Yang et al., 2020). Despite growing evidence of lithological heterogeneity in mantle sources, it is challenging to trace distinctive lithological signatures in magmas. For decades, research has focused on investigating the mantle melting processes by understanding the behavior of highly incompatible elements that are very sensitive to melting and differentiation processes, but are not good indicators of variable source mineralogy or lithology (e. g., Hofmann, 1997; Kelemen et al., 1998). Lambart et al. (2013) reviewed the melting phase relations of pyroxenites and showed that the extreme variability of the pyroxenite melts and the compositional overlap between peridotite and pyroxenite melts make major elements poor markers for the presence of pyroxenites in the source. Additionally, even when the presence of lithological heterogeneity can be demonstrated, estimated proportions of the different lithologies can vary considerably with the compositions of the lithologies, the fate of the melts during magma transport, and the thermal structure of the mantle (Mallik et al., 2021).

First Row Transition Elements (Sc, Ti, V, Cr, Mn, Fe, Co, Ni, Cu, and Zn; hereafter referred to as FRTEs) are thought to be good tracers of mineralogical variation due to their compatible to slightly incompatible nature within the main mantle minerals, causing their ratios to be minimally affected by partial melting and metasomatism (Humayun et al., 2004; Le Roux et al., 2010). Because of this, FRTEs are good

E-mail address: sarah.lambart@utah.edu (S. Lambart).

<sup>\*</sup> Corresponding author.

candidates for the preservation of mineralogical characteristics of mantle source. Le Roux et al. (2011) experimentally determined the mineral/melt partitioning coefficients of FRTEs and concluded that melts produced by clinopyroxene- (cpx) and garnet- (gnt) rich lithologies have lower Mn/Fe, Mn/Zn, and higher Zn/Fe ratios than melts produced by peridotite lithologies.

While the origin of pyroxenites can vary (e.g., Downes, 2007), their presence in the asthenospheric mantle, as well as their compositional diversity, can be primarily attributed to the subduction of the oceanic lithosphere (e.g., Allègre and Turcotte, 1986) and its subsequent modifications (e.g., Herzberg, 2011). Additionally, mantle pyroxenites exhibit a very large range of compositions and mineral assemblages in comparison to peridotites (Lambart et al., 2013). However, very few studies have addressed the systematic distribution of FRTEs across minerals found in natural mantle lithologies (e.g., O'Reilly and Griffin, 1995; Stosch, 1981). Hence, it is essential to characterize the FRTE behavior in natural samples, pyroxenites and peridotites, in order to understand their chemical behavior in the mantle sources of magmas.

In this study, we take a "Big Data approach", compiling analyses performed on natural pyroxenite and peridotite samples from a variety of volcanic and orogenic settings, together with new high-precision analyses of pyroxenitic samples from different geological settings. By calculating mineral/mineral partition coefficients (Ds) and exchange coefficients (KDs) for FRTEs, we examine if natural samples can be used to complement experimental data, by providing a more extensive range of compositions and P-T conditions than covered in experimental studies. We show large datasets of natural samples, despite inevitably including samples in disequilibrium and various levels of analytical precision and accuracy, can produce accurate exchange coefficients. Each pair of mineral shows distinct FRTE exchange coefficients that appear to be independent of temperature and composition, making them reliable input parameters in mantle melting models. To support our conclusions, we present a simple inverse model in which the exchange coefficients calculated in this study are used to constrain the mineralogy of the mantle sources for two basaltic series showing contrasted FRTE ratios: a basaltic series from the Western Volcanic Zone of Iceland (Eason et al., 2015) and a basaltic series from Samoa (Beunon et al., 2020).

# 2. Methods

# 2.1. Database compilation

Natural pyroxenite and peridotite bulk (Fig. S1) and mineral compositions were downloaded from the Interdisciplinary Earth Data Alliance (IEDA)'s EarthChem-PetDB online database (from here on, referred to as the EarthChem databases, Tables S1 & S2). For pyroxenites, we selected analyses from pyroxenites, clinopyroxenites, orthopyroxenites, eclogites and websterites. For peridotites, we selected analyses from dunites, wehrlites, harzburgites, and lherzolites. Samples are from alpine massifs, ophiolites, and mantle xenoliths. We downloaded bulkrock and mineral data separately but under the same selection criteria. Bulk-rock compositions were mainly used to confirm rock types provided by the EarthChem database and to estimate the FRTE ratios of the mantle source used in Section 5. Only data that contained one or more analyses for FRTEs were considered. Samples from both the mineral and bulk-rock datasets with weight percent totals less than 90% were systematically removed before any additional filtering. Compositions falling outside of the three standard deviations envelope calculated on each dataset were also excluded.

For the mineral database, in addition to the filtering described above, we limited our selection to data collected with an Electron MicroProbe (EMP) or Laser-Ablation Inductively Coupled Plasma Mass Spectrometry (LA-ICP-MS). We furthered filtered out EMP analyses with less than 0.01 wt% and LA-ICP-MS analyses lower than 1 ppm. When both EMP and LA-ICP-MS analyses were reported, we used the concentration acquired

through LA-ICP-MS. After plotting mineral analyses from the database, it was clear from visual inspection that numerous outliers existed within multiple orders of magnitude from the mean concentration of samples. For these outliers, their respective source literature was examined. We only discarded analyses if there were there were obvious signs of extensive alteration or if the corresponding data were inaccurately reported in the database.

# 2.2. New analyses

To examine the intrasample variability (i.e., grain-to-grain variations), we analyzed various natural pyroxenites for major elements and FRTEs. Our analyses span samples from volcanic fields and ultramafic massifs: the three samples from Beni Bousera (Morroco) are mantle pyroxenites (e.g., Pearson et al., 1993); the two samples from Chino Valley (Arizona) are arclogites (Rautela et al., 2020), respectively. Results are also compared with analyses performed on seven pyroxenite xenoliths from the San Carlos Reservation, Arizona (labeled SC-()), recently analyzed with the same set up in Lambart et al. (2022).

The samples labeled BB-() originate from the Beni Bousera massif in northern Morocco, and are composed of deformed porphyroblasts set in a fine-grained and often foliated matrix of largely pyroxenitic mineralogy. BB-C-P contains large euhedral porphyroblasts of garnet surrounded by a groundmass composed mainly of clinopyroxene with smaller amounts of amphibole and orthopyroxene (Fig. S2). BB-OP-1 comprises large and heavily deformed clinopyroxene and orthopyroxene with extensive exsolution features surrounded by a fine recrystallized groundmass. BB-Cor is unique in its mineralogy as it contains corundum, among other minerals such as clinopyroxene, garnet, and plagioclase. Corundum is present as large porphyroblasts in a groundmass of isotropic and medium-grained euhedral clinopyroxene and slightly larger garnet crystals. The Chino Valley samples (labeled CV-) are arclogite xenoliths found within a shallow intrusive unit and is composed mainly of clinopyroxene and garnet. CV-4 is foliated and show apparent mineral segregation with layer enriched in clinopyroxene. CV-16 shows a similar mineralogy but no foliation or mineral segregation. For a more detailed description of the Chino Valley xenoliths, please refer to Smith et al. (1994).

We analyzed major and minor element concentrations of minerals from thin sections on the University of Utah's Cameca SX-100 electron microprobe using the two-step approach described in Lambart et al. (2022). We also determined trace element concentrations of the pyroxenes from selected San Carlos xenoliths previously investigated by Lambart et al. (2022). Analyses were performed at the University of Utah on a Teledyne-Photon Machines Analyte Excite Excimer Laser Ablation system attached to an Agilent 8900 ICP-MS on  $\sim 5 \ \text{mm}$  thick polished billets.

Details on the analytical techniques can be found in the Supplementary Material (Text S2). The modes of the samples analyzed in this study are reported in Table S3. Mineral compositions obtained with microprobe and LA-ICP-MS in this study are reported in Tables S4-S6.

# 2.3. Experimental data

To compare natural samples with published experimental data, we used the experimental dataset reported in Mallik et al. (2021) (see Fig. 6.4 in their manuscript) and added experimental results from Mallmann and O'Neill (2009), Regula (2020), Liu et al. (2014), and Holycross and Cottrell (2022). Mn concentrations in selected experimental charges from Lambart et al. (2009, 2013) were reanalyzed using high-current microprobe analyses following the Lambart et al. (2022) analytical setup and are also included in this dataset. Only experiments in which cpx and at least another solid phase were present were considered.

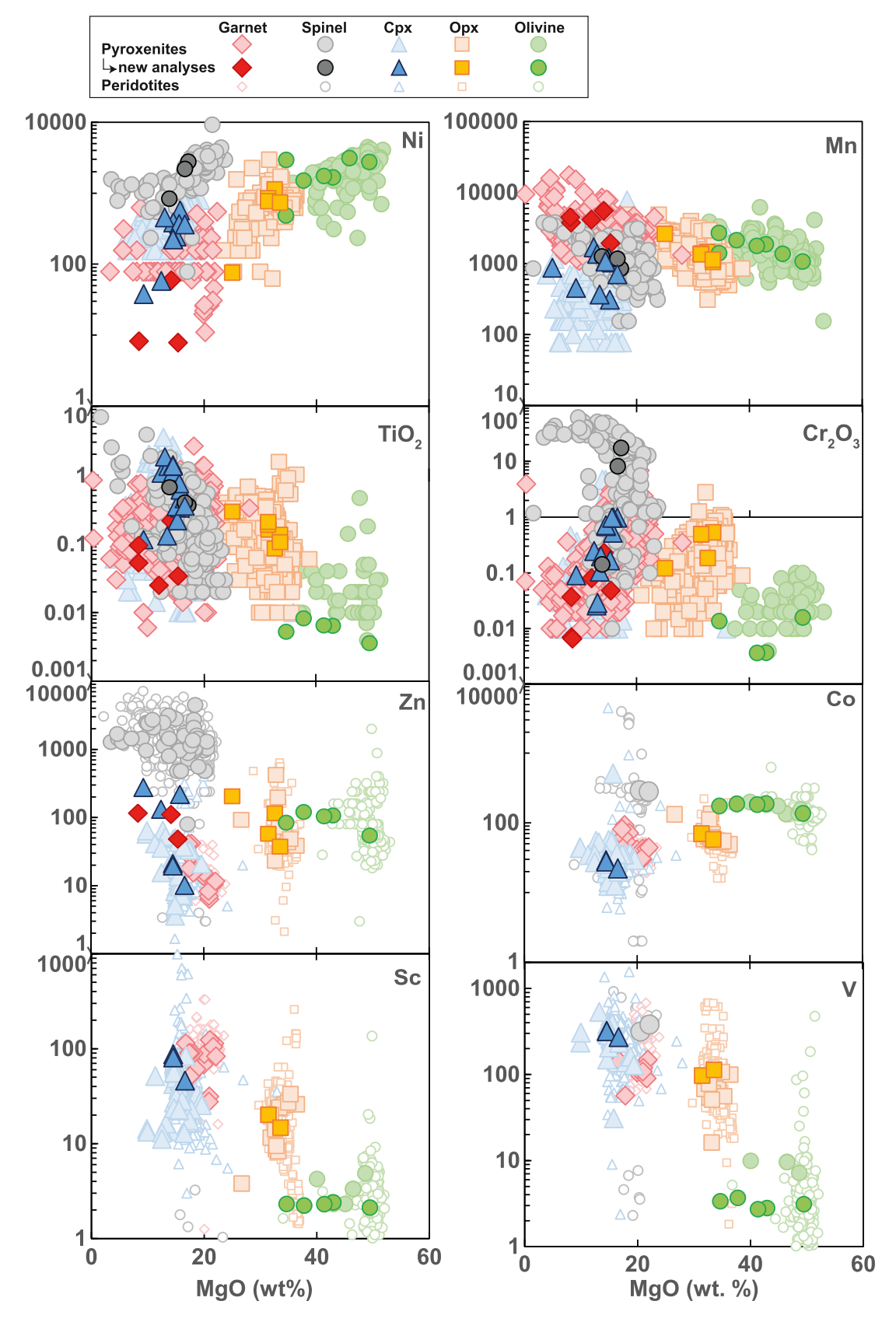


Fig. 1. FRTE concentrations (oxides are in wt%, elements are in ppm) as a function of MgO content in olivine, clinopyroxene, orthopyroxene, garnet, and spinel in pyroxenites (solid symbols). Darker symbols are mineral averages of samples analyzed in this study and in Lambart et al. (2022). For Zn, Co, Sc and V, data on peridotites (small open symbols) are also plotted. Peridotite data for Ni, Mn,  $TiO_2$  and  $Cr_2O_3$  are plotted in Fig. S3. Only LA-ICP-MS analyses were considered for V to avoid EPMA interference between  $TiO_2$  and  $V_2O_5$  (e.g., Snetsinger et al., 1968).

#### 2.4. D and K<sub>D</sub> calculations

Because clinopyroxene is the most common mineral between peridotite and pyroxenite datasets, it was used as a reference mineral for all calculations. Here, the partition coefficient is defined by the ratio of concentration between a mineral and cpx:

$$D_i^{min/cpx} = \frac{C_i^{min}}{C_i^{cpx}} \tag{1}$$

with C, the concentration, and i denoting the FRTE of interest. We calculated each partition coefficient using the representative analyses for each mineral in each sample reported in the EarthChem database. We used the same methods for the average mineral composition in each xenolith analyzed in this study and applied error propagation to calculate the partition coefficient uncertainties for new microprobe and laser analyses, following:

$$errD_{min/cpx} = D_{min/cpx} \sqrt{\left(\frac{errC_{min}}{C_{min}}\right)^2 + \left(\frac{errC_{cpx}}{C_{cpx}}\right)^2}$$
 (2)

with errC representing the two standard deviation on the average concentration.

Mineral exchange coefficients are defined by:

$$K_{D_{j/i}^{\min/cpx}} = \frac{D_{j}^{\min/cpx}}{D_{i}^{\min/cpx}} = \frac{\left(C_{j/C_{i}}\right)^{\min}}{\left(C_{j/C_{i}}\right)^{cpx}}$$
(3)

We also estimated the intrasample variability in the pyroxenite samples analyzed in this study by calculating  $K_Ds$  corresponding to every possible pair of minerals for a given sample (see Section 4.2.2). Finally, in Figs. 6 and 7, experimental Ds and  $K_Ds$  were directly calculated from experiments containing both solid phases. However, this was only doable for  $K_Ds$  for which such experiment exists (mostly Mn/Fe). Most partitioning experiments report equilibrium between a melt and a single solid phase and require the use of several experiments to estimate the

min-min exchange coefficients (see Section 4.2.3).

#### 3. Results

# 3.1. Mineral FRTE concentrations for pyroxenites

In this section, we describe the range of FRTE concentrations in the main minerals present in mantle lithologies: clinopyroxene, orthopyroxene, garnet, olivine and spinel. Within the EarthChem database, the other phases present are mainly feldspar, amphiboles, and Ti-rich oxides. These minerals either contain too few analyses or are inconsistently analyzed across different elements and will not be discussed further.

# 3.1.1. Pyroxenes

Clinopyroxene mineral analyses are the most abundant across both datasets. Compared to the other minerals within the database collection, clinopyroxenes have both low Ni (mostly <1000 ppm) and low Mn (mostly <2500 ppm) concentrations (Fig. 1). Clinopyroxenes also contain lower FeO (mainly <11 wt%) and Co contents (< 60 ppm) than any other considered minerals. V and Sc concentrations are highly variable from  $\sim\!0$  ppm to  $\sim\!500$  and  $\sim\!90$  ppm, respectively. Except for Ni and  $\text{Cr}_2\text{O}_3$  that broadly increase with MgO, and V that broadly decreases, we do not observe any systematic trends between FRTE concentrations and the MgO content in cpx. We note that Zn contents obtained in this study are higher than the concentrations reported in the literature for pyroxenitic clinopyroxene but fall in the range of concentrations observed in peridotites.

Compared to clinopyroxenes, orthopyroxenes show higher Ni, Co, Mn and, to a lesser extent, Zn contents (Fig. 1). V (<60 ppm) and Sc (<35 ppm) concentrations are significantly lower in opx than in cpx. Cu data are sparse and concentrations are below 15 ppm.

FRTE ratios of cpx and opx are similar but cpx ratios span a broader range (Fig. 2). The main differences are for the Co/Fe and Ni/Co ratios which are slightly lower in cpx and higher in in opx, respectively, and are a direct reflection of the higher Co content in opx than in cpx (Fig. 1).

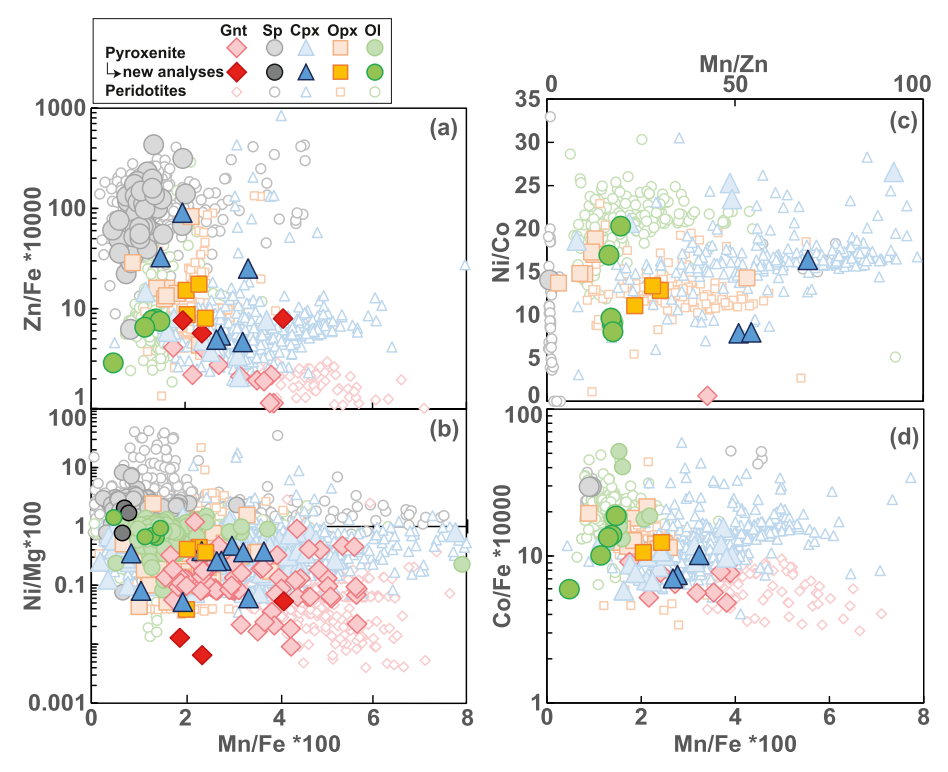


Fig. 2. FRTE ratios in minerals from pyroxenites and peridotites. The colour and symbol scheme follows that in Fig. 1.

#### 3.1.2. Garnet

Garnet contains the highest concentrations of MnO (often exceeding 1.0 wt% in the EarthChem dataset) and Sc (up to 125 ppm), and the lowest Ni contents (generally <500 ppm, Fig. 1).  $\rm Cr_2O_3$  concentration in garnet from pyroxenites remains relatively close to zero up to 20 wt% MgO, but shows a drastic increase up to ~10 wt% when MgO reaches 20 wt% (Fig. 1). Co contents (~30–95 ppm) are slightly higher than those in cpx. They are very few available data on Cu and they are all below 10 ppm. Finally, Zn concentrations in garnet are very similar to those in cpx. In comparison to pyroxenes, garnets present Mn/Fe ratios that expand to higher values, but show lower Ni/Mg, Zn/Fe, Co/Fe (and Ni/Co) ratios (Fig. 2).

#### 3.1.3. Olivine

Data on olivine from pyroxenite are scarce. Olivine contains Ni contents up to  $\sim\!4500$  ppm, which positively correlate to the MgO concentrations. In comparison to other minerals, olivine also has high Co concentrations (up to  $\sim\!400$  ppm). Furthermore, Mn broadly decreases with MgO and Ni contents, staying mostly below 5000 ppm. Finally, olivine has the lowest Cr<sub>2</sub>O<sub>3</sub>, TiO<sub>2</sub>, Sc and V contents of the mineral considered. There is no data on Zn content in olivine whithin the pyroxenite database, but our new analyses reveal concentrations similar to garnet. Zn concentrations in olivine from peridotites are below 400 ppm.

Mn/Fe\*100 ratios plot mostly between 1 and 2, but some samples show ratios up to 8. Ni/Mg\*100 are mostly <2. Zn/Fe ratios are similar to those observed in pyroxenes. On the contrary, Co/Fe ratios are overall significantly higher in olivine than pyroxenes with ratios up to 53 in pyroxenites (Fig. 2).

# 3.1.4. Spinel

Spinel Ni and Mn vs. MgO trends mimic those for olivine, but at lower MgO contents (Fig. 1).  $\rm Cr_2O_3$  and Zn are particularly enriched in spinel with concentrations up to 60 wt% and  $\sim$  5000 ppm, respectively. Spinel also has the highest concentrations in Co (up to  $\sim$ 300 ppm) and Cu (up to 35 ppm). Ranges of V and  $\rm TiO_2$  concentrations are similar to those in cpx. There are only few data for Sc but they suggest very low contents ( $\sim$ < 1 ppm). Spinel presents a very large range of  $\rm Zn/Fe^*10^4$  ratios up to 250 in pyroxenite samples (Fig. 2). On average, spinels also have higher Ni/Mg, and to a lesser extent, Co/Fe ratios than the other minerals. On the contrary, spinel analyses show low Mn/Fe, Mn/Zn and Ni/Co ratios (Fig. 2).

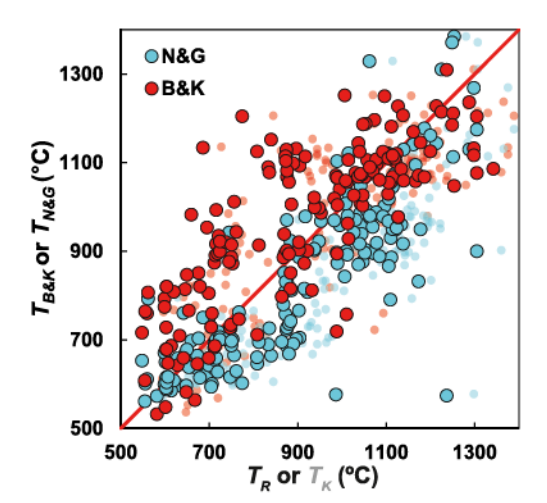


Fig. 3. Comparison of calculated temperatures using Ravna (2000)'s ( $T_R$  - large symbols) and Krogh (1988)'s ( $T_K$  - small light symbols) cpx-gnt geothermometer, with Nimis and Grütter (2010)'s opx-gnt thermometer ( $T_{N\&G}$ ) and Brey and Köhler (1990)'s opx-cpx thermometer ( $T_{B\&K}$ ).

#### 3.2. Geothermometer calculations

Temperatures for the EarthChem database samples were calculated using three geothermometers:

1) For samples containing both clinopyroxene and garnet, we used the Ravna (2000)'s cpx-gnt geothermometer (Eq. (4)), that is a modified formulation of the Ai (1994) geothermometer. Ai's thermometer is based on the high temperature dependence of K<sub>DFe/Mg</sub> first proposed by Ellis and Green (1979), with later modifications accounting for nonlinear K<sub>DFe/Mg</sub> variations with X<sub>Ca</sub><sup>Cnt</sup> and Mg#<sup>Gnt</sup> (Krogh, 1988; Pattison and Newton, 1989), respectively. This new formulation also accounts for K<sub>DFe/Mg</sub> cpx/gnt's' dependence on X<sub>Mn</sub><sup>Cnt</sup> in Mn enriched lithologies and was calibrated using a more comprehensive experimental dataset:

$$T_{R}(K) = \left[ \left( 1939.9 + 3270 \text{ X}_{Ca}^{Gnt} - 1396 \left( X_{Ca}^{Gnt} \right)^{2} + 3319 X_{Mn}^{Gnt} - 3535 \left( X_{Mn}^{Gnt} \right)^{2} + 1105 Mg \#^{Gnt} - 3561 \left( Mg \#^{Gnt} \right)^{2} + 2324 \left( Mg \#^{Gnt} \right)^{3} + 169.4P \right) / \left( \ln K_{D}_{Fe/Mg}^{Gnt/Cpx} + 1.223 \right) \right]$$

$$(4)$$

Krogh's thermometer Krogh (1988) is sometimes preferred over Ravna's as its accuracy was confirmed in experimental work of Brey and Köhler (1990). However, using one or the other thermometer does not influence the discussion below (Fig. 3).

 For samples containing orthopyroxene and garnet, we used Nimis & Grütter's opx-gnt thermometer (2010, Eq. (5)):

$$T_{N\&G}(K) = \left[ 1215 + 17.4P + 1495 \left( X_{Ca}^{gnt} + X_{Mn}^{gnt} \right) / \left( \ln K_{D_{Fe/Mg}}^{opx/gnt} + 0.732 \right) \right]$$
(5)

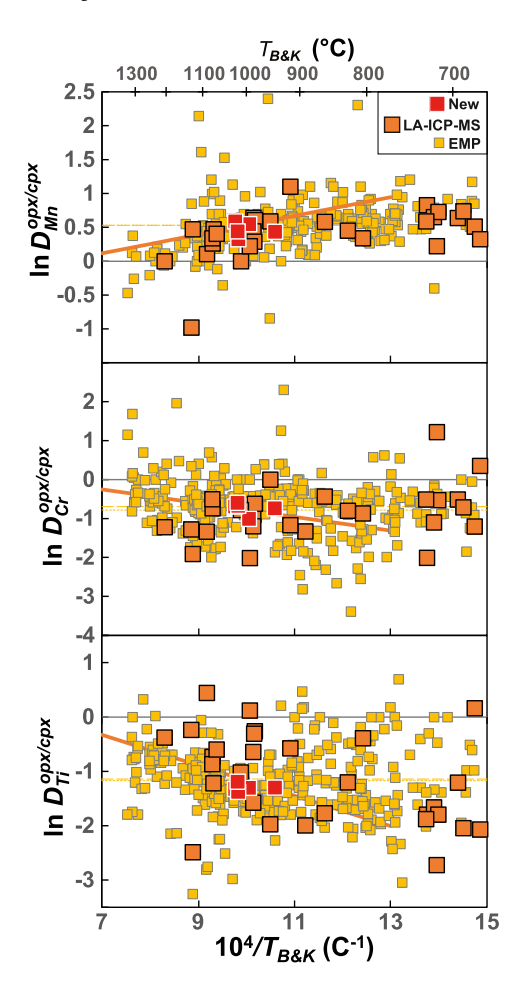
 For samples containing both pyroxenes, we used the opx-cpx Ca—Mg exchange thermometer from Brey and Köhler (1990):

$$T_{B\&K}(K) = \frac{23664 + (24.9 + 126.3(1 - \text{Mg}\#^{\text{cpx}}))P^*10}{13.38 + (\ln{\text{K}_{\text{D}}}^*)^2 + 11.59(1 - \text{Mg}\#^{\text{opx}})}$$
(6)

where 
$${K_D}^{\star} = \frac{1 - N_{Ca}^{cpx} / (1 - N_{Na}^{cpx})}{1 - N_{Ca}^{opx} / (1 - N_{Na}^{opx})}$$

 $X_{Ga, Mn}^{Gat}$  are the molar ratios of Ca or Mn in garnet (Eqs. (4) and (5)), respectively; Mg#s are the molar ratios Mg/(Mg + Fe), assuming all Fe as Fe<sup>2+</sup> (Eqs. (4) and (6));  $N_{Ga, Na}^{epx, opx}$  are the number of cations (Ca or Na) in cpx or opx per formula unit of six oxygens (Eq. (6)). For all three equations, the pressure, P, is in GPa and assumed equal to 1.5 GPa. Changing the pressure by  $\pm 0.5$  GPa changes  $T_R$  by  $\pm 58$  K,  $T_{N\&G}$  by  $\pm 40$  K and  $T_{B\&K}$  by  $\pm 10$  K.

Fig. 3 compares the three thermometers. There are significant discrepancies between them: overall, calculated TB&K plot significantly higher than  $T_R$ . Inversely,  $T_{N\&G}$  are usually lower than  $T_R$ . The lower  $T_{N\&G}$  may be partly explained by the sensitivity of this thermometer to the incorporation of Fe<sup>3+</sup> (Matjuschkin et al., 2014). However,  $T_R$  and  $T_{N\&G}$  are not significantly affected by the presence of Fe<sup>3+</sup> and the discrepancies are too large to be solely explained by an effect of pressure. Cooling rate and tectonic settings can also affect the calculated temperatures as different thermometers likely record different closure temperatures (e.g., Liang et al., 2013; Sun and Lissenberg, 2018). Calibrations of the thermometers must also be taken into account. For instance,  $T_{B\&K}$  was calibrated on four-phase peridotites and temperature > 800 °C. Extrapolation to lower temperatures or for other phase assemblages and compositions may result in poor temperature estimations. Finally, mineral phases are not necessarily all in equilibrium in a given sample and the calculated temperatures might not reflect the temperatures of equilibration, an important consideration when



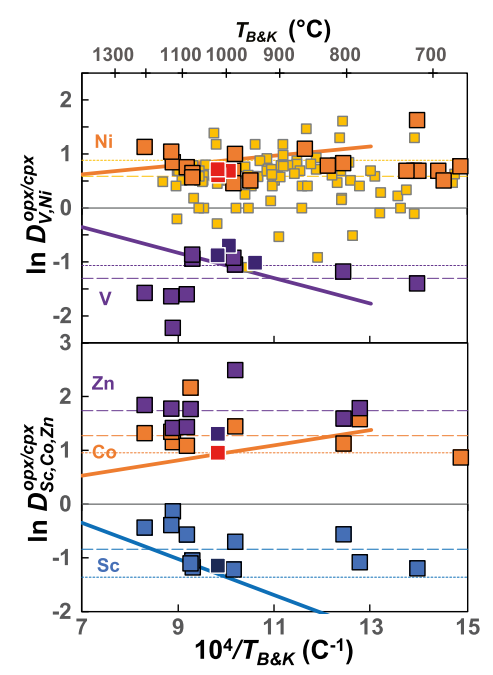


Fig. 4. FRTE partition coefficients between opx and cpx as a function of the calculated reciprocal temperatures of pyroxenites using Brey and Köhler (1990)'s opx-cpx thermometer. The white-contoured squares are the new analyses reported in this study and in Lambart et al. (2022). The solid lines represent the correlations between  $D_{FRTE}^{opx/cpx}$  and temperature obtained by Seitz et al. (1999) (see Fig. S4 for details). Pressure is assumed equal to 1.5 GPa for both datasets. The dotted and dashed lines represent the average  $D_{FRTE}^{opx/cpx}$  obtained from the Seitz et al.'s dataset and from the global pyroxenite dataset (i.e., using both EMP (small squares) and LA-ICP-MS analyses (large squares)), respectively.

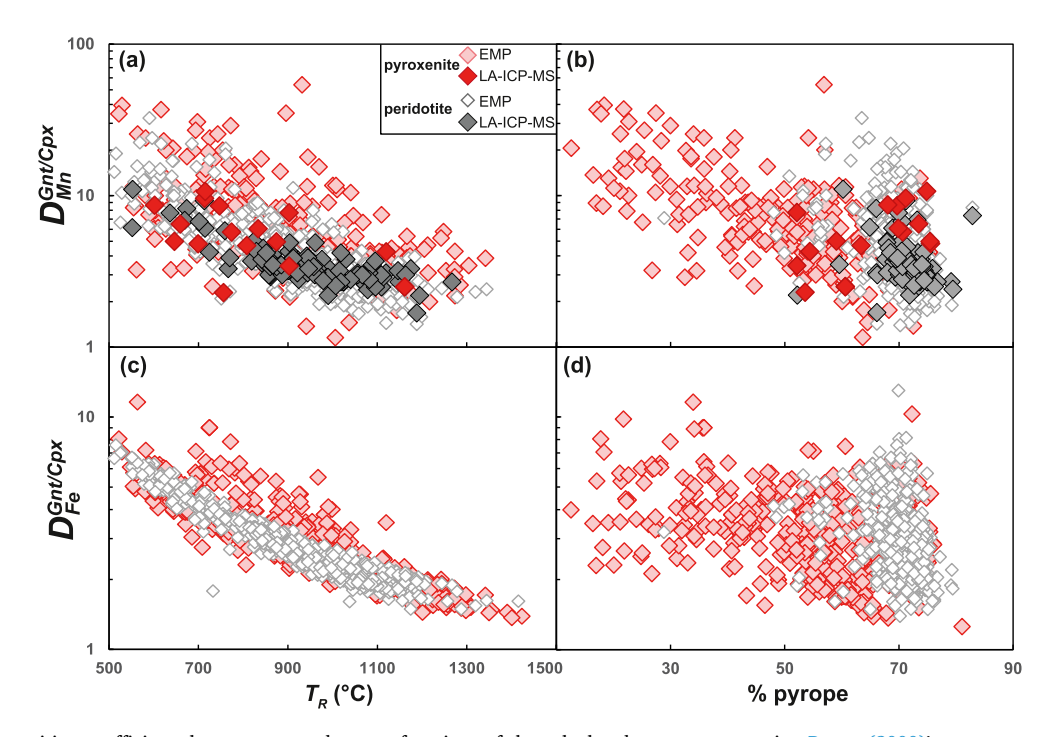


Fig. 5. Mn and Fe partition coefficients between grt and cpx as functions of the calculated temperatures using Ravna (2000)'s cpx-gnt geothermometer ( $T_R$ ) in pyroxenite and peridotite assemblages (a,c) and of the pyrope component in the garnet (b,d).

discussing our results.

#### 4. FRTE partition and exchange coefficients

Some FRTEs are present as trace elements in mantle minerals. Therefore, we can express their behavior based on their partitioning between mantle phases. However, other FRTEs, notably Fe, Mn, Cr, and Ti, are often present as major or minor elements within common mantle minerals (Fig. 1). Because of their higher concentrations, these FRTEs are the most commonly analyzed across petrographic studies. In the supplementary material (see Text S1), we briefly review the underlying crystal chemistry that controls the incorporation of these elements into their respective mineral sites.

# 4.1. Mineral-cpx FRTE partition coefficients

In Fig. 4, we plotted  $D_{FRTFS}^{opx/cpx}$  as a function of  $T_{B\&K}$  calculated from the global pyroxenite dataset and from LA-ICP-MS analyses only. In both cases, there is no apparent correlation. Yet, it is known from several studies that the partitioning of, at least some, transition elements between minerals in mantle lithologies is controlled by temperature (e.g., Bodinier et al., 1987; Hervig and Smith, 1982; Hervig et al., 1986; Stosch, 1981; Witt-Eickschen and O'Neill, 2005; Witt-Eickschen et al., 2009). In fact, Seitz et al. (1999) performed a detailed study on a set of previously described and well-equilibrated xenoliths including garnet and spinel peridotites and garnet websterites. They show a strong temperature dependence between the  $D^{opx/cpx}$  and  $T_{B\&K}$  for Sc, V, Cr, Co and Mn. For comparison, we added on Fig. 4, the trends defined by the samples described in Seitz et al. (1999), assuming P = 1.5 GPa (see Fig. S4 for details). Strikingly, the new pyroxenites investigated in this study and in Lambart et al. (2022) fall very close or on the trends defined by Seitz et al. (1999).

Similarly, the only significant correlations between T and  $D_{FRTE}^{ent/cpx}$  are

for Fe and Mn (Figs. 5 and S4). The peridotite dataset seems to show a slight positive correlation between T and  $D_{Ni}^{ent/cpx}$ , but the correlation is not observed in the pyroxenite dataset (Fig. S5). However, such correlation was previously observed in pyroxenite and eclogite suites (O'Reilly and Griffin, 1995).

The lack of correlation with temperature in the pyroxenite compilation could be due to the significantly larger compositional variability of pyroxenites in comparison to peridotites (e.g., Lambart et al., 2013). In fact, Dupuy et al. (1980) attributed  $D_{Co}^{min/min}$  and  $D_{Sc}^{min/min}$  variations between pyroxenes, garnet, and olivine to mineral composition variations, rather than temperature. Furthermore, Witt-Eickschen and O'Neill (2005) showed a dependence of  $D_{Sc}^{opx/cpx}$  on the pyroxenes Mg# and warned that empirical partitioning relationships should not be extrapolated to different compositions. Stosch (1981) also suggested that the temperature dependencies for  $D_{FRTE}^{ol/cpx}$ ,  $D_{FRTE}^{opx/cpx}$ , and  $D_{FRTE}^{sp/cpx}$  were governed by major element compositions. Finally, the presence of volatiles can also affect the partition coefficients of FRTEs. Witt-Eickschen et al. (2009) showed that hydrous peridotite xenoliths have higher values of  $D_{T_i}^{ol/cpx}$  and  $D_{T_i}^{ol/opx}$  than expected for anhydrous xenoliths. In fact, Ti is preferentially found in tetrahedral sites in anhydrous olivine, but can also be incorporated into M1 crystallographic sites under hydrous conditions (e.g., Cherniak and Liang, 2014; see Text S1.2).

To test this hypothesis, we examined numerous chemical parameters (e.g., mineral Mg#, Ca#, Na $_2$ O content of cpx, % pyrope in garnet, spinel Cr#). The only apparent correlation we observed is between

 $D_{Mn}^{ent/cpx}$  and the garnet composition:  $D_{Mn}^{ent/cpx}$  broadly decreases with the increasing pyrope component in the pyroxenite dataset (Fig. 5b). As Mn preferentially substitutes for Fe rather than Mg, this could reflect the calibration of Ravna's thermometer that is dependent of the garnet Mg#, a proxy for the pyrope/almandine ratio (Eq. (4)). However, this dependence is not supported by the strong correlation

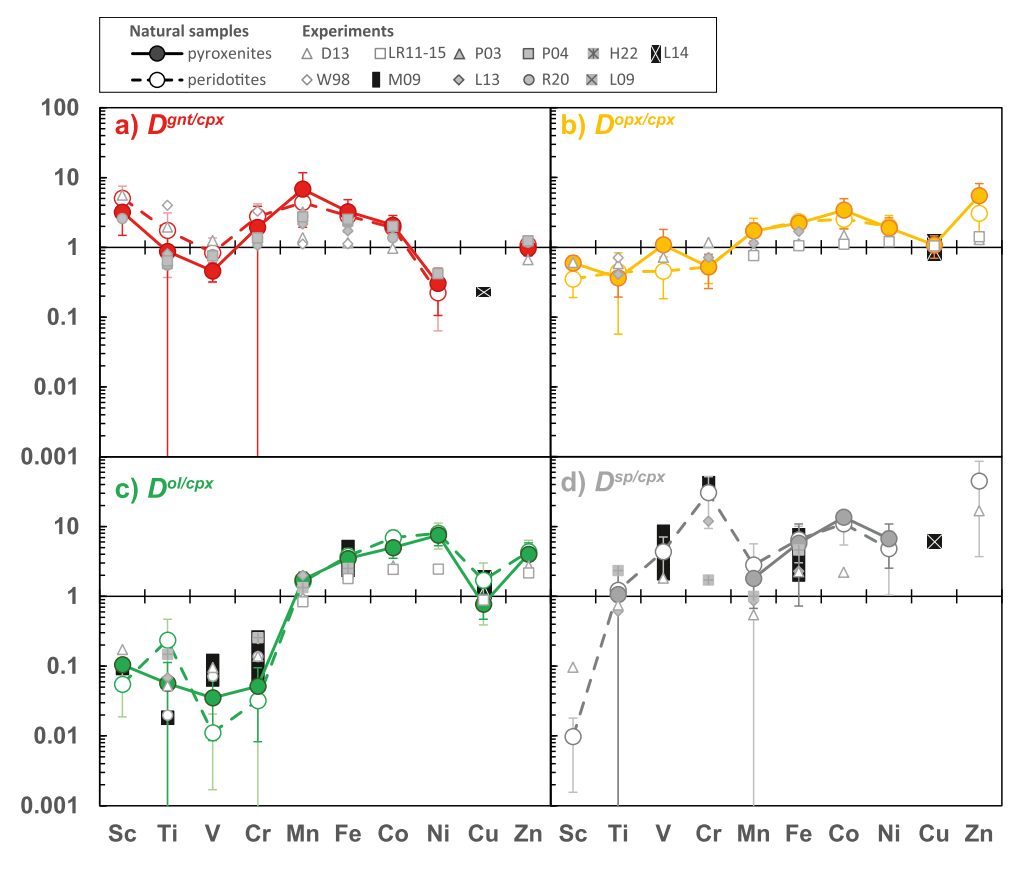


Fig. 6. Average partition coefficients calculated from natural samples (including our new analyses, large circles) and experiments (small light symbols) for FRTEs in pyroxenite (solid symbols) and peridotite (open symbols) samples. The error bars represent one standard deviation on natural pyroxenite and peridotite data. Data source for experiments are as follows: D13: Davis et al., 2013; H22: Holycross and Cottrell, 2022; L09: Lambart et al., 2009; L13: Lambart et al., 2013; L14: Liu et al., 2014; LR11-15: Le Roux et al., 2011, 2015; P03: Pertermann and Hirschmann, 2003a; P04: Pertermann et al., 2004; R20: Regula, 2020; W98: Walter, 1998. In (c) and (d), M09 represents the range of Dol/cpx for Sc, Ti, V, Cr and Fe with  $f_{O_2}$  varying between QFM - 5 and QFM + 5 (Mallmann and O'Neill, 2009).

between  $T_R$  and  $D_{Fe}^{gnt/epx}$  in the peridotite dataset (Fig. 5c) despite the restricted range of pyrope content (Fig. 5d). Additionally, when only LA-ICP-MS data are considered, the dependence of  $D_{Mn}^{gnt/epx}$  to the temperature is preserved (Fig. 5a), but no correlation is observed between the pyrope content and  $D_{Mn}^{gnt/epx}$  (Fig. 5b). The compilation of natural samples did not produce other noticeable correlations with temperature (Fig. S5) or composition.

The overall lack of apparent correlation between  $D_{FRTES}^{min/cpx}$  and temperature could be explained if some FRTE partitioning behaviors were insensitive to temperature, but is more likely attributed to the fact that the compilation included samples that are not well equilibrated (Fig. 3). Hence, large compilations of natural samples cannot be used to quantitatively determine the FRTEs partition coefficients for a given condition as the effects of temperature cannot be properly assessed.

Despite the significant scatter observed in Fig. 4, data are broadly consistent with FRTE Ds between opx and cpx defined by Seitz et al.'s trends. For FRTEs with large datasets (Mn, Ti, Cr, and to a lower extent Ni), there is also an excellent consistency of the average partition coefficients calculated from both datasets (i.e., the EarthChem pyroxenite dataset and Seitz et al.'s dataset). Similarly, there is an excellent overlap for  $D_{RRT/S}^{min/cpx}$  between the pyroxenite and the peridotite datasets (Figs. 5, S5). With the consistency of average  $D_{RRT/S}^{min/cpx}$  between peridotite and pyroxenite datasets and between natural and experimental samples (Fig. 6), we can qualitatively compare the partitioning behaviors of FRTEs between various minerals and clinopyroxene. For instance, the partitioning behavior of FRTEs between opx and cpx can be described as:

$$D_{Ti,Sc,V,Cr}^{opx/cpx} < 1 \sim D_{Cu}^{opx/cpx} < D_{Mn,Ni}^{opx/cpx} < D_{Co,Zn}^{opx/cpx}$$

The temperature dependence observed in Seitz et al. (1999) can also explain most offsets between average  $D_{FRTEs}^{\text{opx/cpx}}$  values obtained from natural samples and the experimentally determined coefficients (Fig. 6). In fact, the experimental partition coefficients for heavy FRTEs (i.e., Mn to Zn) are overall lower than the partition coefficients obtained on natural data. This is consistent with the negative correlations observed for Mn, Ni and Co between temperature and  $D^{\mathrm{opx/cpx}}.$ Inversely, natural partition coefficients for Cr and Ti are lower than experimental ones, consistent with the correlation observed by Seitz et al. for these two elements (Fig. 4). The strong contrast between the temperatures of natural samples and the experimental temperatures might explain why such dependence is apparent here and not among the natural samples.

The distribution of FRTEs between olivine and cpx is similar to their distribution between opx and cpx in that the distribution changes from preferentially partitioning into clinopyroxene (Sc to Cr) to partitioning into olivine (Mn to Ni & Zn) with decreasing atomic radius. However, the FRTE partitioning behavior between olivine and clinopyroxene is significantly more fractionated than between pyroxenes (Fig. 6). The valency of Fe, Cr and V can vary over the range of oxygen fugacities ( $f_{O_2}$ ) and might affect their partitioning behavior. V/Sc in basalts, for instance has been used as a proxy for magma  $f_{O_2}$  (e.g., Lee et al., 2005), since V becomes increasingly incompatible with increasing  $f_{O_2}$ , while the partition coefficient of Sc stays constant. The effect of  $f_{O_2}$  is discussed more in details in Text S1.5. Mallmann and O'Neill (2009) investigated the role of oxygen fugacity on the partitioning behavior of a series of elements, including Sc, Ti, V, Cr and Fe. In Fig. 6c, we plotted the range they obtained for  $D^{ol/cpx}$  with  $f_{O_2}$  conditions relevant for Earth (i.e., QFM - 5 to QFM + 5; Mallmann et al., 2021).  $D_{Sc,Ti}^{ol/cpx}$  are relatively constant but  $D_{V,Cr}^{ol/cpx}$  decrease with increasing fugacity. The dependence of  $D_{V,Cr}^{ol/cpx}$  to oxygen fugacity however does not change the relative partitioning behavior of Cr and V in olivine as the maximal values reported by Mallmann and O'Neill (2009) (for QFM - 4.7) are still lower than the values reported for the other minerals. Data on Cu are very limited, but natural datasets and experiments (Le Roux et al., 2015; Liu et al., 2014) both suggest a partition coefficient close to 1, similar or lower than  $D_{Mn}$ . In addition,  $D_{Cu}^{ol/cpx}$  obtained from natural samples should be considered

as a maximum value as the presence of micro-inclusions of sulfide can increase the analyzed Cu content in olivine (e.g., Lambart et al., 2022). Zn concentrations in olivine and cpx analyzed in this study show homogeneous distributions through the grain, and the Ds calculated from our samples are consistent with a strong fractionation of Zn ( $D_n^{ol/cpx} \sim 4$ ).

Except for Ni, all divalent cations reported in natural samples preferentially partition into garnet over clinopyroxene, with  $\mathcal{D}_{Mn,Sc}^{ent/cpx}$  showing the highest values. Ni is not easily incorporated in garnet because of the large difference in crystal field stabilization energy for this element in the distorted cubic site of garnet, compared to the octahedral sites in olivine, clinopyroxene and orthopyroxene (e.g., Ross et al., 1996). No partitioning data are reported for  $\mathcal{D}_{Cu}^{cut/cpx}$ . Only two experiments with both garnet and cpx were reported in Liu et al. (2014) suggesting a low partition coefficient, similar to Ni. In comparison, Ti, Cr and V, all that occupy the Y crystallographic sites, and show relatively neutral partitioning behavior:

$$D_{Ni,Cu}^{gnt/cpx} < 1 \sim D_{Ti,V,Zn}^{gnt/cpx} < D_{Cr,Fe,Co}^{gnt/cpx} < D_{Sc,Mn}^{gnt/cpx}$$

Spinel data are limited for natural samples, and uncertainties on partition coefficients are higher than for other Ds. Nevertheless, all FRTEs but Sc seem to preferentially partition into spinel over cpx with  $D_{\rm Zh,\ Cr,\ Co}^{\rm sp/cpx} > 10$  (Fig. 6).

Overall, heavy FRTEs are relatively incompatible in cpx in comparison to other minerals (i.e.,  $D_{Mn}^{min/cpx} = 1$ ), except for Ni that is particularly incompatible in garnet. The partitioning behavior of light FRTEs

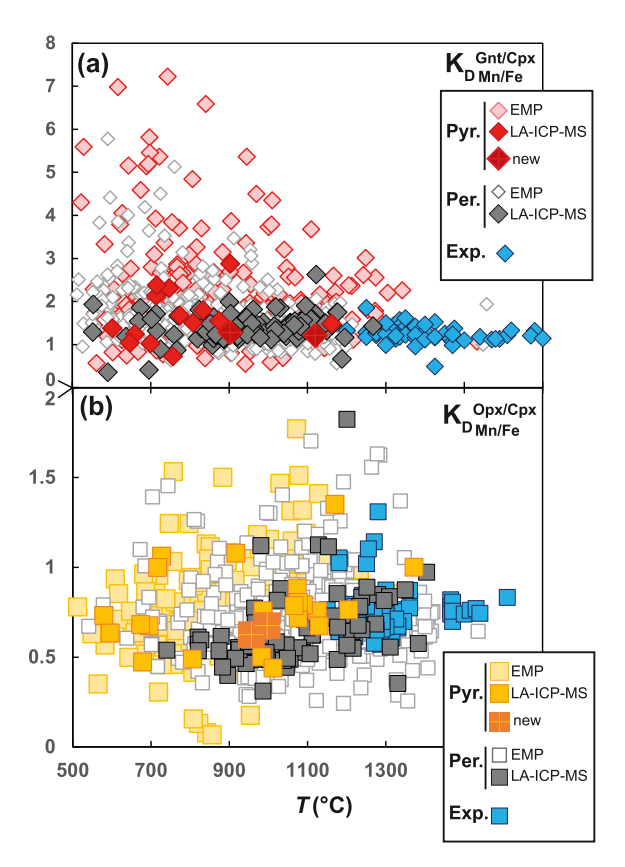


Fig. 7. Mn—Fe exchange coefficients between garnet (a) or opx (b) and cpx as a function of temperature. Temperatures of natural peridotites (Per.) and pyroxenites (Pyr.) samples are calculated with Ravna's Gnt-Cpx thermometer (2000) in (a) and Brey & Köhler's Opx-Cpx thermometer (1990) in (b). For experimental data (Exp.), the reported temperature is the experimental temperature. Data source for experiments: Baker and Stolper, 1994; Davis et al., 2013; Lambart et al., 2009, 2013; Laporte et al., 2014; Le Roux et al., 2011; Pertermann and Hirschmann, 2003a; Pertermann et al., 2004; Pickering-Witter and Johnston, 2000; Schwab and Johnston, 2001; Walter, 1998; Wasylenki et al., 2003.

(i.e., Sc to Cr) is more variable. Sc and Ti favor garnet. V is particularly incompatible in olivine but behaves similarly in garnet, clinopyroxene, orthopyroxene, and spinel. Finally, Cr preferentially partitions into spinel and garnet and, to a lesser extent, cpx, rather than in opx or olivine.

#### 4.2. Exchange coefficients

#### 4.2.1. Effect of temperature and lithology

It is challenging to evaluate the impact of temperature and composition on  $K_Ds$  because of the lack of apparent correlation between most  $D_{\rm FRTE}^{\rm pex}$  and calculated temperatures. However, results presented by Le Roux et al. (2011) and supported by Mallik et al. (2021), suggest that the FRTE exchange coefficients between mineral and liquid ( $K_D^{\rm min}/$ ) are independent of the bulk composition, lithology, and MgO content of the melt, a proxy for the temperature.

As described above,  $D_{Mn}^{min/cpx}$  and  $D_{Fe}^{min/cpx}$  are two partition coefficients for which the correlation with temperatures of equilibration is apparent in both the peridotite and the pyroxenite datasets (Figs. 4, 5). Hence, if  $K_D^{min/cpx}$  was a function of temperature, the correlation between  $K_{D_{Mn/Fe}}^{min/cpx}$  and temperature of equilibration would likely be preserved. Such correlation is not observed (Fig. 7), suggesting that

 $K_D^{\rm min/cpx}$  are indeed independent of temperature, consistent with Le Roux et al. (2011) and Mallik et al. (2021)'s conclusions.

With the EachChem interface, it is not possible to simultaneously download the mineral compositions and their associated bulk rock composition. Despite this, lithology types are broadly correlated with the bulk composition (Fig. S1). Eclogites show high Al<sub>2</sub>O<sub>3</sub> and low MgO contents, clinopyroxenites show high CaO contents, and orthopyroxenites and websterites have low CaO and high MgO contents. Peridotites, in comparison, show a much narrower range of bulk compositions and plot as a MgO-rich end-member on the trends defined by the pyroxenites (e.g., Lambart et al., 2013). It is worth noting that "eclogite" and "clinopyroxenite" terms are sometimes used indiscriminately in the literature. Additionally, the terms "pyroxenite" and "peridotite" prevent investigating the effect of the mineral assemblage (and indirectly, bulk composition) on the partitioning behavior of FRTEs among these two groups. Nevertheless, in Fig. S6, we plotted the same dataset as in Fig. 7, but we distinguished the different lithologies. While the  $K_{D_{Mn/Fe}}^{\phantom{Mn/Fe}}$  in eclogite and clinopyroxenite shows more scatter, there is no systematic variation of K<sub>D</sub>s with lithology.

In Fig. 8, we plotted the Mn/Fe and Ni/Mg values in minerals as a function of their respective ratios in clinopyroxene, calculated using the pyroxenite and the peridotite datasets. These two ratios were chosen due

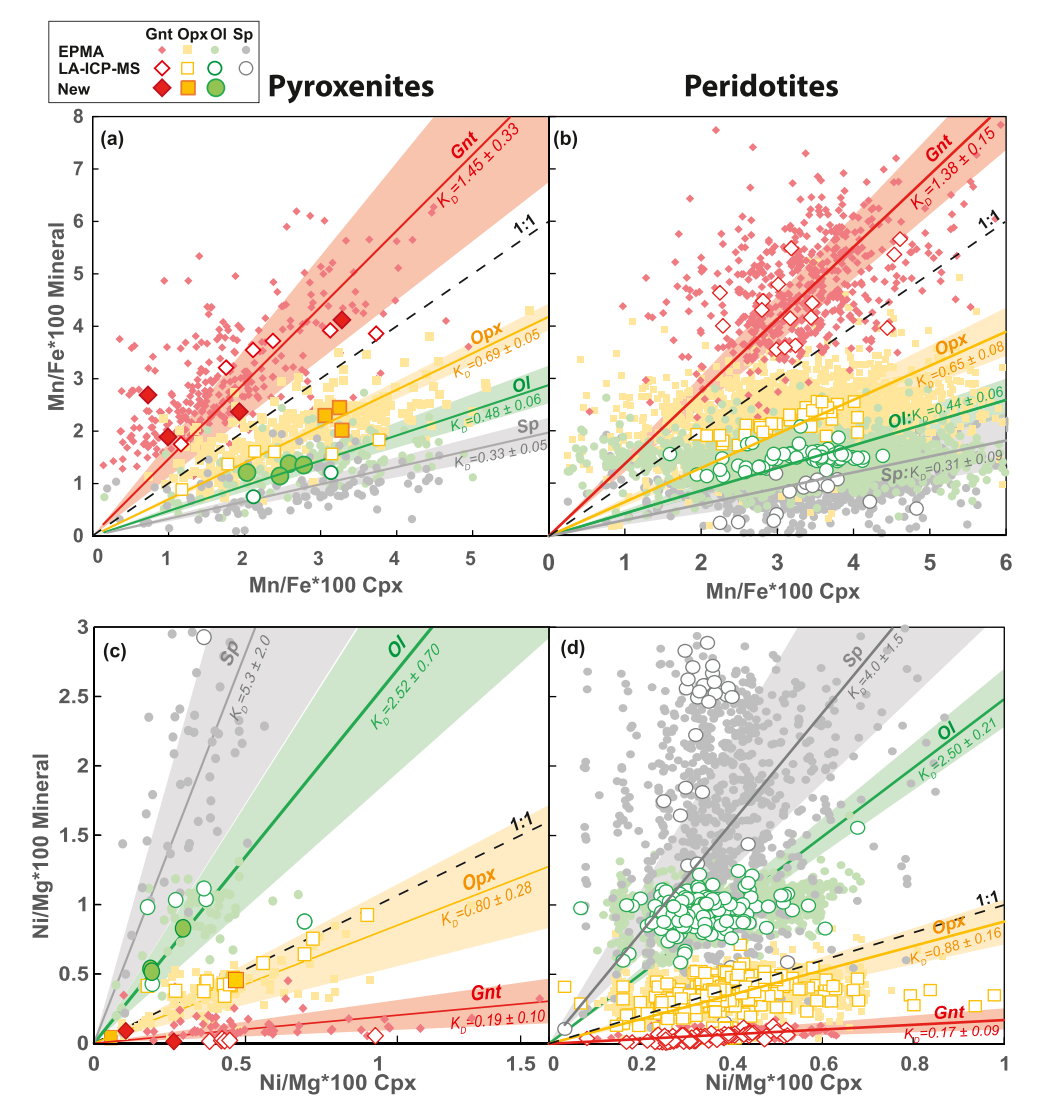


Fig. 8. Mn/Fe\*100 ratios (a-b) and Ni/Mg\*100 ratios (c-d) in minerals as a function of the ratios in cpx for the pyroxenite (left) and peridotite (right) datasets. Linear regressions (solid lines) represent the exchange coefficients for the respective mineral pairs, following Eq. (3). The envelopes represent the respective two-standard deviation. In (a) and (c) the larger darker symbols are averages of samples analyzed in this study and in Lambart et al. (2022).

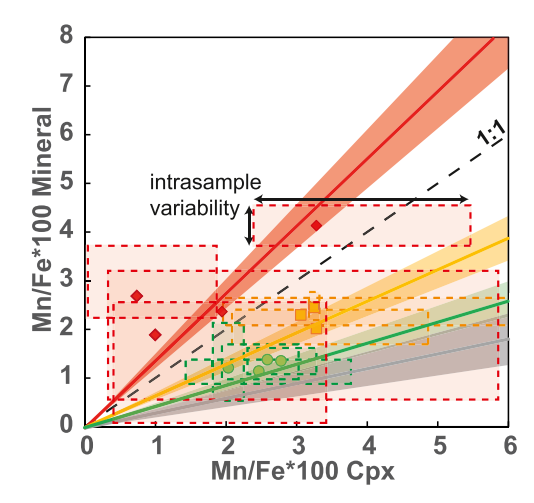


Fig. 9. Mn/Fe\*100 ratios for minerals analyzed in this study and in Lambart et al. (2022). Averages for each pyroxenite sample are represented by symbols (red diamond = gnt-cpx pair, orange squares = opx-cpx pair, green circles = olivine-cpx pairs). The intrasample variability for each pair is represented by the dashed outlined boxes. Colored envelopes are the  $K_D \pm 2\sigma$  range for all-natural data (i.e., same error given in Table 1). (For interpretation of the references to colour in this figure legend, the reader is referred to the web version of this article.)

to the abundance of analyses for these four elements in our datasets. As  $K_Ds$  are independent of temperature, following Eq. (3), we can use these plots to calculate the exchange coefficients for various pairs of minerals. Unlike Fig. 7, where values of  $K_Ds$  were calculated for each sample,  $K_Ds$  obtained in Fig. 8 represent average values for each pair of minerals (following the approach used in Le Roux et al., 2011), allowing for more efficient estimations of uncertainty. All  $K_{D_{Mn/Fe}}$  for pyroxenites are distinct from one another within two standard deviations and decreases from  $K_{D_{Mn/Fe}}$  to  $K_{D_{Mn/Fe}}$  (Fig. 8a). Additionally,  $K_{D_{Mn/Fe}}$  values obtained from the peridotite dataset (Fig. 8b) are consistent with the pyroxenite  $K_{Ds}$  (Fig. 8a). Similar observations can be done when comparing the  $K_{D_{NU/Mg}}$  (Fig. 8c-d). The consistency between the FRTE  $K_{Ds}$  obtained from the pyroxenite and the peridotite dataset suggests, once again, that  $K_{Ds}$  are independent of the source lithology and consequently of the bulk composition.

#### 4.2.2. Precision versus number of analyses

Fig. 9 shows the intrasample variability we obtained on K<sub>D</sub>s for samples analyzed in this study and in Lambart et al. (2022). Despite using high precision analytical techniques, carefully avoiding cracks or inclusions, and working with relatively fresh samples (Fig. S2), we report high intrasample variability across all of the analyzed pyroxenite samples. This variability reflects intrasample disequilibrium and clearly demonstrates that partition and exchange coefficients cannot be obtained from a single pair of minerals in a given natural sample. However, in Fig. 4, our average  $D^{opx/cpx}$  fall close to or on the trends defined by Seitz et al. (1999). This suggests that, at least for these samples, grain-tograin FRTE disequilibrium occurs on a small scale (i.e., cm-scale) and averaging numerous analyses in a given sample can provide a value close to the equilibrium between two solid phases. This is also supported by the fact that the same samples fall in the two-standard deviation envelope defined for each KD in Fig. 9. Yet, several of the analyzed samples (e.g., CV4) display mineral composition that fall outside of the error envelope. This suggests that the number of samples, and the sample diversity, are, at least, as important as the amount and precision of analyses.

Table 1
Recommended values for mineral/cpx FRTE exchange obtained calculated from natural samples compared with the calculated experimental coefficients.\*

			gnt	opx	ol	sp
Mn/Fe	Natural data	K <sub>D</sub>	1.39	0.65	0.44	0.31
		$2\sigma$	0.15	0.08	0.06	0.09
		n	909	3973	2912	2336
	Le Roux 2015	$K_D$	1.12	0.72	0.47	0.31
		$2\sigma$	0.35	0.05	0.02	0.04
Zn/Fe	Natural data	$K_D$	0.40	1.28	1.31	12.00
		$2\sigma$	0.04	0.2	0.19	5
		n	30	89	313	37
	Le Roux 2015	$K_D$	0.49	1.31	1.37	8
		$2\sigma$	0.28	0.22	0.24	2
Co/Fe	Natural data	$K_D$	0.66	0.97	1.73	2.5
		$2\sigma$	0.07	0.19	0.15	0.9
		n	102	226	562	54
	Le Roux 2015	$K_D$	0.73	1.17	1.32	2.12
		$2\sigma$	0.16	0.26	0.22	0.98
Mn/Zn	Natural data	$K_D$	2.82	0.44	0.28	0.01
		$2\sigma$	0.74	0.11	0.09	0.02
		n	77	188	307	53
	Le Roux 2015	$K_D$	2.32	0.55	0.34	0.22
		$2\sigma$	0.22	0.08	0.06	0.06
Ni/Mg	Natural data	$K_D$	0.17	0.88	2.5	4
		$2\sigma$	0.09	0.16	0.21	1.5
		n	343	2895	4789	1165
	Le Roux 2015	$K_D$				
		$2\sigma$				
Ni/Co	Natural data	$K_D$	0.07	0.78	1.26	0.77
		$2\sigma$	0.15	0.1	0.13	0.16
		n	85	234	507	53
	Le Roux 2015	$K_D$	0.19	1.18	0.98	0.11
		$2\sigma$	0.38	0.7	0.5	0.06
Ni/Sc	Natural data	$K_D$	0.02	7.1	128	
		$2\sigma$	0.02	3	52	
		n	229	245	237	
	Le Roux 2015	$K_D$	0.09	5	14.6	8.3
		$2\sigma$	0.18	2.6	12.4	4.2

 $<sup>^*</sup>$  Experimental coefficients were calculated from the recommended  $D_{FRTE}^{min/melt}$  in Le Roux et al. (2015). See Text S3 for details.

The number of analyses performed by LA-ICP-MS per sample (and per phase) is usually much smaller than the number of analyses performed by EMP. If a sample shows grain-to-grain variation, the analyses reported might not be representative of the mineral average concentration in the sample. Hence, we argue that a high number of analyses should be preferred over a low number of high-precision analyses to obtain a good estimation of the FRTE ratios at phase equilibrium. In Table 1, we report the calculated value of  $K_{\rm D_{\rm FRTES}}$  using combined datasets, allowing the largest number of samples to be considered. The accuracy of exchange coefficients derived from natural samples obtained from less than 40 mineral pairs must be, however, evaluated cautiously.

# 4.2.3. Comparison with experimental data and recommended exchange coefficients

We used the recommended values for min-melt partition coefficients  $(D_{RRTE}^{min/melt})$  reported in Le Roux et al. (2015) to calculate experimental min-cpx exchange coefficients  $(K_{DRTES}^{min/cpx})$ . The calculations for the coefficients and their associated standard deviation are detailed in Text S3 and the experimental coefficients are reported in Table 1. With the exception of coefficients involving Ni, the coefficients obtained in this study overlap with the experimental ones. In particular,  $K_{D_{NNSC}}^{ol/cpx}$  derived from natural samples is an order of magnitude higher than the experimental coefficient. Ni is well known for diffusing outside of the capsule during experimental runs (e.g., Filiberto and Treiman, 2009; Matzen et al., 2013). Hence, we are confident that the natural exchange coefficients involving Ni are more reliable than those derived from experiments.

Another issue with using experimental min-melt partition coefficients (Dmin/melt), such as those presented in Le Roux et al. (2015), to calculate min-cpx exchange coefficients is that the various  $D^{min/melt}$ s are derived from experiments performed at different pressure and temperature conditions and with various starting materials. The FRTE exchange coefficients considered in this study are independent of temperature and composition, but partition coefficients are not. Hence ratios of  $D^{min/melt}$ obtained at different conditions might introduce errors in the estimation of the  $D^{min/cpx}$ . These uncertainties can then propagate in the calculations of  $K_D^{min/cpx}$ , adding to the analytical error (Text S3). Such an effect is hard to quantify. This would not be a major problem if the partition coefficients were highly contrasted, but that is not the case for FRTEs who all behave as compatible to moderately incompatible elements during partial melting of mafic and ultramafic systems. Hence, the standard deviation reported in Table 1 for the experimental exchange coefficients are likely underestimated.

The two-standard deviations calculated from Le Roux et al. (2015)'s dataset are overall similar or larger than the error calculated from natural samples. Hence, we argue that, when available, the exchange coefficients derived from a sufficiently high number of natural samples (>40) are more reliable than exchange coefficients indirectly derived from experiments performed in various conditions. However, this study also highlights the need for multi-mineral experiments in which  $K_D s$  can be obtained from two coexisting solid phases.

# Application: a new approach for constraining the Earth's mantle heterogeneity

For the last three decades, the most common modeling approach used to determine the proportion of lithological heterogeneity in the mantle has been to consider a mantle in which the composition and/or mineralogy of different lithologies are fixed (e.g., Brown and Lesher, 2014; Elkins et al., 2019; Hirschmann and Stolper, 1996; Lambart, 2017; Lambart et al., 2019; Le Roux et al., 2011; Mallik et al., 2021; Shorttle and Maclennan, 2011; Sobolev et al., 2007; Yang et al., 2020). However, the main limitation of these models is also the main input parameter: the composition (chemical or mineralogical) of each lithology present in the mantle must be known and must stay constant. Both of these assumptions have been recently challenged. In fact, using an inverse method, Brown et al. (2020) suggested that the trace element composition of the pyroxenite component in the mantle source of Iceland significantly differs from the composition of a subduction-modified recycled oceanic crust commonly used in forward models. More recently, Mourey et al. (2022) looked at FRTE concentrations in magmatic olivines produced at the Kılauea Volcano (Hawaii) between 1500 and the 2018 eruption. The evolution of the olivine composition cannot be explained by a change of the pyroxenite fraction in the mantle, but would rather reflect an increase of the modal proportion of clinopyroxene in the mantle source. Hence, rather than assuming the nature of the different lithologies potentially present in the mantle, here we developed a new approach to determine the bulk mineralogical make-up of the mantle using FRTE experimental partition coefficients and K<sub>D</sub>s obtained in this study on natural samples (Table 1).

#### 5.1. Strategy

We constructed a simple modal batch melting model and compared the results with two separate basalt suites: A subglacial basalt suite from the Western Volcanic Zone (WVZ) in Iceland (Eason et al., 2015) and a compilation of Oceanic Island Basalts (OIBs) from Samoa (Beunon et al., 2020). We chose these two suites because of their contrasted average Mn/Fe and Zn/Fe ratios (Fig. S7) and their relatively primitive nature (MgO >7.5 wt%). We estimated the melt composition using an equation modified from the modal batch melting equation:

$$\left(\text{Mn/Fe}\right)_{\text{liq}} = \left(\text{Mn/Fe}\right)_0 * \frac{1 + F\left(\frac{1}{D_{\text{Fe0}}} - 1\right)}{K_{\text{D0}} + F\left(\frac{1}{D_{\text{Fe0}}} - K_{\text{D0}}\right)} \tag{7}$$

where (Mn/Fe)<sub>0</sub> is the ratio in the mantle source,  $K_{D0}$  is the bulk exchange coefficient between solid and the melt,  $D_{Fe0}$  is the bulk partition coefficient for iron between the solid and the melt and F is the melt fraction.  $K_{D0}$  is obtained using cpx/melt exchange coefficients from the experimental literature and the min/cpx exchange coefficients from this study (Table 1). An example is described below for Mn/Fe:

$$K_{D\,Mn/Fe}^{\,gnt/melt} = \left(K_{D\,Mn/Fe}^{\,gnt/melt}\right)_{experiment} {}^*\!\left(K_{D\,Mn/Fe}^{\,gnt/cpx}\right)_{natural} \tag{8a}$$

K<sub>D0</sub> is expressed as:

$$K_{D0} = \sum X_{min} K_{DMn/Fe}^{min/melt}$$
(8b)

with  $X_{min}$  being the fraction of the mineral of interest in the source, and  $\sum X_{min} = 1$ .

We applied the same equation for Zn/Fe. We used the partition coefficients for Fe determined by Davis et al. (2013). The values used for the exchange coefficient between cpx and melt are  $K_{DMn/Fe}^{cpx/melt}=1.58$  and  $K_{DZn/Fe}^{cpx/melt}=0.68$  (Davis et al., 2013).

We ran our model for both Mn/Fe and Zn/Fe assuming a single mantle lithology. For low to moderate degrees of melting (< 20%), the ratio in the melt stays relatively constant during melting (Text S4 and Fig. S8). We used a scenario in which the mantle is composed of five main mineral phases: olivine, cpx, opx, garnet and spinel. We solved for all the modal proportions in the mantle source that can reproduce the Mn/Fe ratio for the two selected basalt suites. This scenario has nonunique solutions (one equation - 5 variables), so we ran two hundred calculations for both basalt suites, varying the input modal mineralogy. The fraction of olivine, opx, cpx and gt, ranged from 0 to 1. For spinel however, ignoring rare exceptions (e.g., the local presence of chromite), the proportion of spinel in mafic and ultramafic rocks is usually relatively small (i.e., a few percent; e.g., Lambart et al., 2009, 2013; Baker and Stolper, 1994; Laporte et al., 2004, 2014), so we only allowed for the spinel fraction to vary from 0 and 0.05 (0.05 is generally considered a maximum modal value for peridotite; e.g., Eggins et al., 1998). The 200 input mineral proportions used in calculations are plotted in Fig. S9. We reproduce the same calculations using Zn/Fe ratios. For both sets of calculations, the chosen values for the ratios of the source are the averages between the medians obtained from the EarthChem pyroxenite and peridotite databases ((Mn/Fe)<sub>0</sub> = 0.0181 and (Zn/Fe)<sub>0</sub> =  $8.39*10^{-4}$ ; Fig. S10). These values are consistent with the ratios of the primitive mantle (Mn/Fe  $_{pyrolite} = 0.017 \pm 0.002$  and Zn/Fe  $_{pyrolite} = 8.8$  $\pm 1.6*10^{-4}$  (McDonough and Sun, 1995).

# 5.2. Modeling results

Fig. 10 presents the results obtained from Mn/Fe and Zn/Fe ratios separately. Results are consistent with the theoretical expectations: the source of the Samoa basalts, that have a lower Mn/Fe ratio and higher

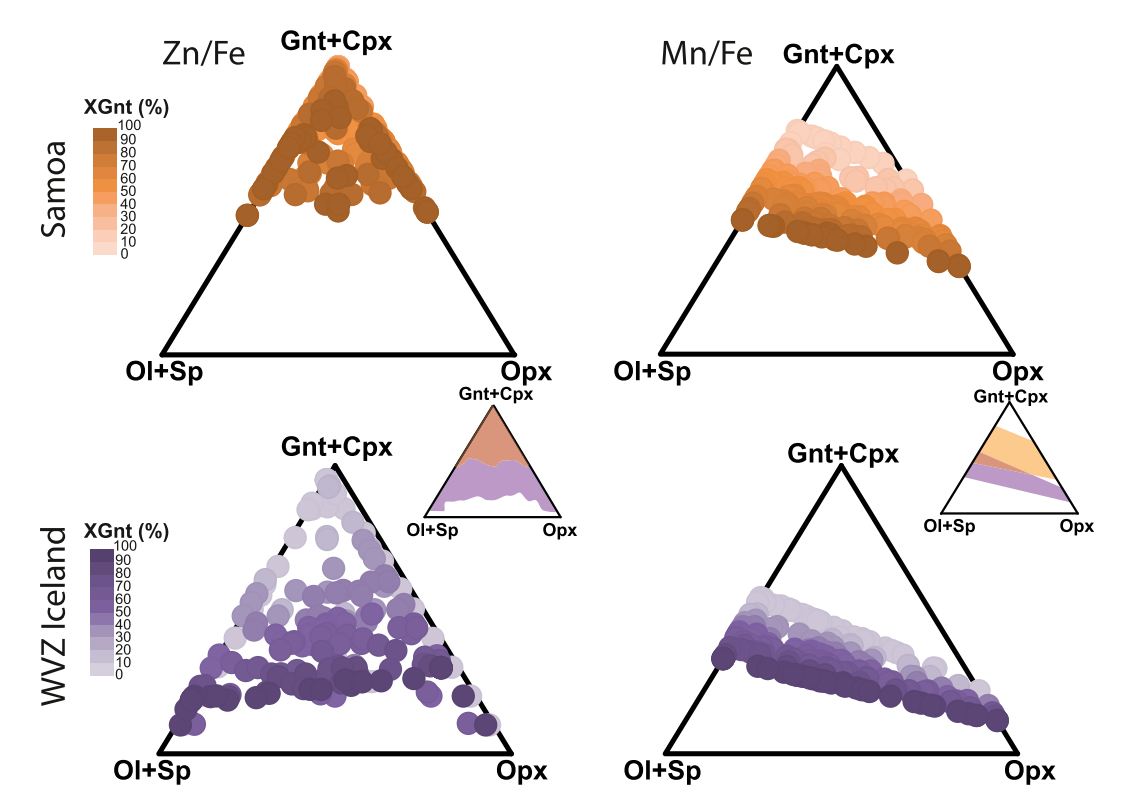


**Fig. 10.** Batch melting model results: output modal source proportions reproducing either the average Zn/Fe ratios (left column) or the Mn/Fe ratios (right column) of the basalt suites from Samoa (top) and the WVZ in Iceland (bottom). The small triangles illustrate the overlap between the two basaltic series for a given ratio. XGnt = Gnt/(Gnt + Cpx). See supplementary Fig. S11 for a projection Gnt-Cpx-Ol+Opx+Sp.

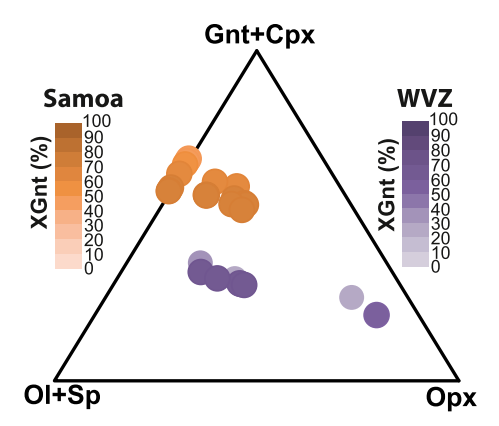


**Fig. 11.** Combined batch melting model results: output modal source proportions reproducing both the average Mn/Fe ratio and the average Zn/Fe ratio of the basalt suites from the Iceland WVZ (purple) and Samoa (yellow). XGnt = Gnt/(Gnt + Cpx).

Zn/Fe ratio than the WVZ Icelandic suite, is richer in garnet and clinopyroxene and requires a lower proportion of olivine and opx (+ spinel) than the Icelandic suite. More importantly, these calculations highlight that a given FRTE ratio in the melt can be reproduced by a large range of modal proportions in the source and that calculations using individual ratios result in potential significant overlap between both basalt series. The range of modal proportions in the source is significantly narrowed down when both ratios are considered together (Fig. 11), resulting in no overlap in mineralogy in the sources between the two different suites. The average modal fraction in the source of the Iceland WVZ basalt suite is 0.30 ol + 0.26 opx + 0.10 cpx + 0.15 gnt + 0.03 sp. In comparison, the average modeled source mineralogy for the Samoan basalt is 0.38 ol + 0.10 opx + 0.16 cpx + 0.36 gnt.

#### 5.3. Proof of concept

The model presented in the previous section can solve for the average mineralogical makeup of the mantle. However, there are several lines of evidence that suggest the mantle is composed of two or more lithologies (Lambart et al., 2016, and reference therein). We propose that the calculations presented here can be used as a first step in modeling the melting of a multi-lithology mantle. To demonstrate the value of such an approach, we ran an additional scenario in which we consider a mantle composed of two lithologies: pyroxenite and peridotite. We then solve for the fraction of pyroxenite in the mantle. For these calculations, we considered that both lithologies have the same bulk Mn/Fe and Zn/Fe, and therefore, the same as the source ratios used in Section 5.2. This choice is discussed in Text S2.

In a first run, the two lithologies in the mantle sources of both basalt suites are the same: the subsolidus modal proportion of the peridotite KR4003 at 3 GPa (Walter, 1998), and the near-solidus modal proportion of the MORB-type eclogite G2 at 3 Gpa (Pertermann and Hirschmann, 2003b). Modal proportions used in calculations are reported in Table S7. Similar "model" lithologies have been used extensively in forward and inverse modeling (e.g., Kimura and Kawabata, 2015; Koornneef et al., 2012; Lambart et al., 2016; Le Roux et al., 2011; Pertermann and Hirschmann, 2003b; Shorttle and Maclennan, 2011; Sobolev et al., 2005, 2007; Yang et al., 2020) independently of the oceanic setting (e.g., thickness of the lithosphere, temperature of the mantle, intraplate vs extension magmatism). Using this combination, we obtained 34% of pyroxenite-derived melt in the source of the WVZ in Iceland and 67% of pyroxenite-derived melt in the source of Samoa Island with the Mn/Fe ratio (Eq. (7)). However, we cannot solve for the Zn/Fe ratio as the Iceland basalt suite requires more than 100% peridotite in its source, while the Samoan basalt suite requires more than 100% pyroxenite component in its respective source lithology (Table S7).

In a second run, we used the results obtained in Section 5.2 as input

parameter to adjust the mineralogical proportions attributed to both lithologies. In fact, results from Section 5.2 show that the source of the WVZ is relatively rich in pyroxenes and must contain a small fraction of spinel to reproduce the low Zn/Fe ratios of the basalts. In comparison, the source beneath Samoa is richer in garnet than the two "model" lithologies used in the previous calculations. For the source of the WVZ, using a more fertile spinel peridotite (i.e., similar to FER-E; Pickering-Witter and Johnston, 2000) and a hybrid garnet pyroxenite similar to KG1 (Kogiso et al., 1998) results in consistent outputs for both sets of calculations: ~49% of the pyroxenite component contribute to magma genesis beneath the WVZ. Conversely, using a more refractory peridotite, and a garnet-rich eclogite (e.g., Kogiso and Hirschmann, 2006) results in both ratios suggesting a pyroxenite contribution close to 64% in the basalts from Samoa.

We highlight that calculations performed in this study provide an estimation of the contribution of the pyroxenite component in the magmas, not an estimation of their proportion in the sources. Estimating their proportions in the sources is beyond the scope of this study (mostly because of the limitations described below) and will be the subject of a future study. Nonetheless, it is interesting to compare our preliminary results with previous works to determine if such a two-step approach would improve the characterization of the nature of the mantle sources. Samoa basalts are thought to preserve the EM2 (Enriched Mantle 2) signature (e.g., Jackson and Dasgupta, 2008). While the nature of this mantle component is debated (e.g., Adams et al., 2021; Jackson et al., 2014; Workman et al., 2004), the number of investigations for the presence of a non-peridotitic lithology in the mantle source of Samoa is still limited. Nevertheless, several recent studies point out the need for the contribution of pyroxenite in Samoa basalt genesis to explain their compositions (e.g., Konter et al., 2016; Mallik et al., 2021; Wang et al., 2021). Our calculations suggest a higher pyroxenite contribution in Samoa basalts (64%) than in Icelandic basalt (49%). A higher contribution can be explained either by a larger fraction in the mantle source (e.g., Mallik et al., 2021), by a higher melt productivity difference between the pyroxenite and the peridotite components (e.g., Lambart et al., 2016), by a smaller contribution of the peridotitic mantle due to a thicker lithospheric lid (e.g., Sobolev et al., 2007), or by any combinations of theses processes. Discriminating between theses variables is not trivial (e.g., Mallik et al., 2021). However, our results show that the bulk mineralogy must be rich in garnet, consistent with the high Gd/Yb of the basalts (Wang et al., 2021). Hence, the presence of a thick lithospheric lid may play an important role in the composition of the Samoa basalts.

In contrast to Samoa, the nature of the pyroxenite component in the mantle source of Iceland has been the subject of many studies (e.g., Brown et al., 2020; Koornneef et al., 2012; Lambart, 2017; Neave et al., 2018; Rasmussen et al., 2020; Shorttle and Maclennan, 2011; Shorttle et al., 2014; Sigmarsson and Steinthórsson, 2007). Consistent with our results, several forward models have suggested the contribution of an olivine pyroxenite, similar to KG1 (Kogiso et al., 1998), in the mantle source of Iceland (e.g., Lambart, 2017; Shorttle and Maclennan, 2011; Shorttle et al., 2014). Our results also highlight the necessity for the presence of spinel in the peridotitic lithology to reach an agreement between the two FRTE ratios. This is consistent with the lower pressure of melting expected beneath Iceland than beneath Samoa. In comparison to KG1, however, our results suggest that the pyroxenite component likely contains a higher proportion of garnet and lower proportion of olivine. Additionally, the previous forward models suggested a lower contribution of the pyroxenite component in the melt for the area (i.e., ~20 to 40% for KG1 lithology; Shorttle et al., 2014) than predicted in this study. In their inverse model, Brown et al. (2020) found an even lower contribution of the pyroxenite component. However, their pyroxenite melt productivity is calibrated with the KG1 lithology. Increasing the garnet/olivine ratio of the pyroxenite component should result in increasing the fertility of the pyroxenite component, consistent with a higher contribution in the magma. We note that it would also require a higher mantle potential temperature or a higher proportion of refractory harzburgite (i.e., not contributing to magma genesis) to preserve the buoyancy of the mantle (Shorttle et al., 2014). Hence, our study demonstrates the benefits of including the bulk mineralogy of the mantle in forward and inverse models, bringing additional constraints to better characterize the nature and the relative proportions of the lithologies present in the mantle source as well as the melting conditions (i.e., mantle potential temperature and final pressure of melting).

# 5.4. Limitations

We highlight that in the last two runs presented above (Section 5.3), we are only testing one possible pair of lithologies for each basalt suite (i.e., the same pair for both suites in the first run and a different pair for each suite, adjusted from the obtained bulk mineralogy, in the second run). Testing each possible pair, or a combination of three or more lithologies, is beyond the scope of this paper and will be the subject of a future publication. Here we simply highlight how taking the bulk mineralogical make-up of the mantle into account can significantly improve the quantification of the different lithologies in the mantle source, eventually required to constrain the abundance and time scales of crustal recycling.

Our melting scenarios contain various assumptions and limitations that are somewhat inherent in developing simple models for complex natural systems. The most obvious might be the use of a batch melting equation rather than fractional or continuous melting. Batch melting is known to reproduce the composition of aggregated fractional melts for highly incompatible elements well (e.g. Hertogen and Gijbels, 1976). However, FRTEs may behave differently. Hence it is important to compare our results with fractional melting. In mantle assemblages, FRTEs are moderately compatible to moderately incompatible. Hence, they are thought to be minimally affected by melting processes (Humayun et al., 2004; Le Roux et al., 2010). To test this assumption, we calculated the compositions of pure peridotite and pyroxenite melts using batch and fractional melting (see Text S4 and Fig. S8a). In up to ~50% of melting, the difference between models is negligible in comparison to the difference of ratios produced by the two lithologies, supporting the statement that FRTE ratios in basalts are mostly affected by the mineralogy of the source. Other assumptions in our model affect the true dispersion of the results, that is the range of bulk mineralogies (or lithologies) capable of reproducing the FRTE ratios of the basalt. Among the chosen input parameters that result in artificially decreasing the scatter of the results in this study are (i) considering the average melt composition rather than the full range of basalt compositions (Fig. S7), (ii) considering that only two lithologies possible lithologies in the source, (iii) using constant FRTE ratios for the mantle source (Figs. S8b and S10), (iv) using constant partition coefficients, and (v) assuming all Fe as Fe<sup>2+</sup> (Text S2.2). Finally, post-melt generation processes, such as fractionation, magma recharge and mixing, and diffusion, may also influence the FRTE ratios of the lavas and associated magmatic olivines. The pressure of fractionation of olivine (Hole, 2018) and magma mixing can affect the Ni content of the crystallizing olivine (Gleeson and Gibson, 2019). Similarly, deep fractionation of augite might result in a decrease of the Mn/Fe ratio in the melt (Vidito et al., 2013). Additional source components, not necessarily accounted for in all melting models may also complicate the interpretation of the results. For instance, the contribution of the lithosphere to the genesis of continental basalts can affect the FRTE ratios in melt and magmatic olivine (Xu et al., 2022). Finally, the presence of accessory phases (e.g., phlogopite, sulfides) in the mantle source might affect the partitioning of some of the FRTEs (e. g., Veter et al., 2017; Usui et al., 2022). However, as proven by the significant improvement that resulted from using two FRTE ratios (Fig. 11) rather than one (Fig. 10), taking into account multiple (>2) FRTEs ratios will further help in reducing the true dispersion of the result.

#### 6. Conclusions and outlook

Given the consistency between experimental and natural datasets and the temperature and lithology independence of  $K_{D_{PRTE}}^{min/cpx}$ s, we propose that natural samples are good candidates for constraining the exchange behaviors of FRTEs in mantle lithologies. We provide a set (Mn/Fe, Zn/Fe, Co/Fe, Mn/Zn, Ni/Mg, Ni/Co, and Ni/Sc) of recommended mineral-cpx exchange coefficients. However, exchange coefficients determined using a small number (< 40) of natural samples should be considered with caution. Hence, we stress the need for additional studies on the partitioning and exchange behavior of the less commonly analyzed FRTEs (Sc, V, Co, Cu, and Zn) through both experimental investigations and analyses of natural samples. Additionally, natural samples provide an alternative for investigating the partition behavior of elements that are challenging to determine (e.g., Ni). Finally, we demonstrate that FRTE exchange coefficients can be used as powerful lithological tracers of the mantle source, but only when combined. Using a simple inverse melting model, we showed that 1) a given FRTE ratio can be reproduced by a large range of source mineralogies, and 2) combining ratios significantly narrows down the output source mineralogy. Such additional constraints on the bulk mineralogy of the mantle can serve as input parameters in models of heterogeneous mantle melting to better characterize the nature and proportion of lithologies present in mantle sources.

# Funding

This work was supported by the National Science FoundationEAR-1946346 grant to S.L.

#### Authors contributions

S.L. designed the study. O.L and S.L. wrote the manuscript, O.L performed the analyses and data treatment under the supervision of S.L.

# Data availability

All the data supporting the findings of this study are included in the manuscript and in the supplementary material attached with this paper.

# **Declaration of Competing Interest**

The authors declare that they have no known competing financial interests or personal relationships that could have appeared to influence the work reported in this paper.

# Data availability

All data supporting the findings of this study are included in the manuscript and in the supplementary material attached with this paper.

# Acknowledgments

We thank the reviewers, Yan Liang and Sally Gibson, for their constructive comments, as well as Sonja Aulbach for her editorial handling, which greatly improved the quality of this manuscript. This study has benefited from discussions with John Bartley, Barb Nash, Ananya Mallik, and Adrien Mourey. For assistance with analytical techniques, we thank Wil Mace (EPMA), Diego Fernandez, Christopher Anderson and Brad Munk (LA-ICP-MS). We also thank George Rossman for the synthetic Mn and Ni olivines used as primary standards in electron microprobe analyses, and Quintin Sahratian for help with sample preparation. The MagMaX group wants to dedicate this paper to Kurt Lawson.

#### Appendix A. Supplementary data

Supplementary data to this article can be found online at https://doi.org/10.1016/j.chemgeo.2022.121137.

#### References

- Adams, J.V., Jackson, M.G., Spera, F.J., Price, A.A., Byerly, B.L., Seward, G., Cottle, J.M., 2021. Extreme isotopic heterogeneity in Samoan clinopyroxenes constrains sediment recycling. Nat. Commun. 12 (1), 1–10.
- Ai, Y., 1994. A revision of the garnet-clinopyroxene Fe<sup>2+</sup> Mg exchange geothermometer. Contrib. Mineral. Petrol. 115, 467-473.
- Allègre, C.J., Turcotte, D.L., 1986. Implications of a two-component marble-cake mantle. Nature 323, 123–127.
- Baker, M.B., Stolper, E.M., 1994. Determining the composition of high pressure mantle melts using diamond aggregates. Geochim. Cosmochim. Acta 58, 2811–2827. https://doi.org/10.1016/0016-7037(94)90116-3.
- Beunon, H., Mattielli, N., Doucet, L.S., Moine, B., Debret, B., 2020. Mantle heterogeneity through Zn systematics in oceanic basalts: evidence for a deep carbon cycling. Earth Sci. Rev. 205, 103-174.
- Bodinier, J.L., Guiraud, M., Fabriés, J., Dostal, J., Dupuy, C., 1987. Petrogenesis of layered pyroxenites from the Lherz, Freychinede and Prades ultramafic bodies (Ariege, French Pyrenees). Geochim. Cosmochim. Acta 51 (2), 279-290.
- Brey, G.P., Köhler, T., 1990. Geothermobarometry in four-phase lherzolites II. New thermobarometers, and practical assessment of existing thermobarometers. J. Petrol. 31 (6), 1353–1378.
- Brown, E.L., Lesher, C.E., 2014. North Atlantic magmatism controlled by temperature, mantle composition and buoyancy. Nat. Geosci. 7, 820–824.
- Brown, E.L., Petersen, K.D., Lesher, C.E., 2020. Markov chain Monte Carlo inversion of mantle temperature and source composition, with application to Reykjanes Peninsula, Iceland. Earth Planet. Sci. Lett. 532, 116007.
- Cherniak, D.J., Liang, Y., 2014. Titanium diffusion in olivine. Geochim. Cosmochim. Acta 147, 43–57.
- Davis, F.A., Humayun, M., Hirschmann, M.M., Cooper, R.S., 2013. Experimentally determined mineral/melt partitioning of first-row transition elements (FRTE) during partial melting of peridotite at 3 GPa. Geochim. Cosmochim. Acta 104, 232–260.
- Downes, H., 2007. Origin and significance of spinel and garnet pyroxenites in the shallow lithospheric mantle: ultramafic massifs in orogenic belts in Western Europe and NW Africa. Lithos 99 (1-2), 1-24.
- Dupuy, C., Dostal, J., Liotard, J.M., Leyreloup, A., 1980. Partitioning of transition elements between clinopyroxene and garnet. Earth Planet. Sci. Lett. 48, 303-310.
- Eason, D.E., Sinton, J.M., Grönvold, K., Kurz, M.D., 2015. Effects of deglaciation on the petrology and eruptive history of the Western Volcanic Zone, Iceland. Bull. Volcanol. 77, 1–27.
- Eggins, S.M., Rudnick, R.L., McDonough, W.F., 1998. The composition of peridotites and their minerals: a laser-ablation ICP-MS study. Earth Planet. Sci. Lett. 154, 53-71.
- Elkins, L.J., Bourdon, B., Lambart, S., 2019. Testing pyroxenite versus peridotite sources for marine basalts using U-series isotopes. Lithos 332, 226-244.
- Ellis, D.J., Green, D.H., 1979. An experimental study of the effect of Ca upon garnetclinopyroxene Fe-Mg exchange equilibria. Contrib. Mineral. Petrol. 71, 13–22.
- Filiberto, J., Treiman, A.H., 2009. The effect of chlorine on the liquidus of basalt: first results and implications for basalt genesis on Mars and Earth. Chem. Geol. 263, 60–68.
- Gleeson, M.L., Gibson, S.A., 2019. Crustal controls on apparent mantle pyroxenite signals in ocean-island basalts. Geology 47 (4), 321–324.
- Hertogen, J., Gijbels, R., 1976. Calculation of trace element fractionation during partial melting. Geochim. Cosmochim. Acta 40 (3), 313–322.
- Hervig, R.L., Smith, J.V., 1982. Temperature-dependent distribution of Cr between olivine and pyroxenes in lherzolite xenoliths. Contrib. Mineral. Petrol. 81 (3), 184–189.
- Hervig, R.L., Smith, J.V., Dawson, J.B., 1986. Petrogenetic and crystallochemical significance of some minor and trace elements in olivine, pyroxenes, garnet and spinel. Trans. R. Soc. Edinb. Earth Sci. 77, 181–201.
- Herzberg, C., 2011. Identification of source lithology in the Hawaiian and Canary Islands: implications for origins. J. Petrol. 52 (1), 113–146.
- Hirschmann, M.M., Stolper, E.M., 1996. A possible role for garnet pyroxenite in the origin of the "garnet signature" in MORB. Contrib. Mineral. Petrol. 124, 185–208.
- Hofmann, A.W., 1997. Mantle geochemistry: the message from oceanic volcanism.

  Nature 385, 219-229.
- Hole, M.J., 2018. Mineralogical and geochemical evidence for polybaric fractional crystallization of continental flood basalts and implications for identification of peridotite and pyroxenite source lithologies. Earth Sci. Rev. 176, 51–67.
- Holycross, M., Cottrell, E., 2022. Experimental quantification of vanadium partitioning between eclogitic minerals (garnet, clinopyroxene, rutile) and silicate melt as a function of temperature and oxygen fugacity. Contrib. Mineral. Petrol. 177 (2), 1–23.
- Humayun, M., Qin, L., Norman, M.D., 2004. Geochemical evidence for excess iron in the mantle beneath Hawaii. Science 306, 91–94.
- Jackson, M.G., Dasgupta, R., 2008. Compositions of HIMU, EM1, and EM2 from global trends between radiogenic isotopes and major elements in ocean island basalts. Earth Planet. Sci. Lett. 276 (1-2), 175-186.
- Jackson, M.G., Hart, S.R., Konter, J.G., Kurz, M.D., Blusztajn, J., Farley, K.A., 2014. Helium and lead isotopes reveal the geochemical geometry of the Samoan plume. Nature 514 (7522), 355-358.

Kelemen, P.B., Hart, S.R., Bernstein, S., 1998. Silica enrichment in the continental upper mantle via melt/rock reaction. Earth Planet. Sci. Lett. 164, 387-406

- Kimura, J. -I., Kawabata, H., 2015. Ocean basalt simulator version 1 (OBS1): Trace element mass balance in adiabatic melting of a pyroxenite-bearing peridotite. Geochem. Geophys. Geosyst. 16, 267-300. https://doi.org/10.1002 2014GC005606.
- Kogiso, T., Hirose, K., Takahashi, E., 1998. Melting experiments on homogeneous mixtures of peridotite and basalt: application to the genesis of ocean island basalts. Earth Planet. Sci. Lett. 162, 45-61. https://doi.org/10.1016/S0012-821X(98)00156-
- Kogiso, T., Hirschmann, M.M., 2006. Partial melting experiments of bimineralic eclogite and the role of recycled mafic oceanic crust in the genesis of ocean island basalts. Earth Planet. Sci. Lett. 249, 188-199. https://doi.org/10.1016/j.epsl.2006.07.016.
- Kogiso, T., Hirschmann, M.M., Pertermann, M., 2004. High-pressure partial melting of mafic lithologies in the mantle. J. Petrol. 45, 2407–2422.
- Konter, J.G., Pietruszka, A.J., Hanan, B.B., Finlayson, V.A., Craddock, P.R., Jackson, M. G., Dauphas, N., 2016. Unusual  $\delta^{56}$ Fe values in Samoan rejuvenated lavas generated in the mantle. Earth Planet. Sci. Lett. 450, 221-232.
- Koornneef, J.M., Stracke, A., Bourdon, B., Meier, M.A., Jochum, K.P., Stoll, B., Grönvold, K., 2012. Melting of a two-component source beneath Iceland. J. Petrol. 53, 127-157. https://doi.org/10.1093/petrology/egr059.
- Krogh, E.J., 1988. The garnet-clinopyroxene Fe-Mg geothermometer a reinterpretation of existing experimental data. Contrib. Mineral. Petrol. 99, 44-48.
- Lambart, S., 2017. No direct contribution of recycled crust in Icelandic basalts. Geochem. Perspect. Lett. 4, 7-12.
- Lambart, S., Laporte, D., Schiano, P., 2009. An experimental study of pyroxenite partial melts at 1 and 1.5 GPa: implications for the major-element composition of Mid-Ocean Ridge Basalts. Earth Planet. Sci. Lett. 288, 335-347.
- Lambart, S., Laporte, D., Schiano, P., 2013. Markers of the pyroxenite contribution in the major-element compositions of oceanic basalts: review of the experimental constraints. Lithos 160, 14-36.
- Lambart, S., Baker, M.B., Stolper, E.M., 2016. The role of pyroxenite in basalt genesis: Melt-PX, a melting parameterization for mantle pyroxenites between 0.9 and 5 GPa. J. Geophys. Res. Solid Earth 121, 5708-5735.
- Lambart, S., Koornneef, J.M., Millet, M.A., Davies, G.R., Cook, M., Lissenberg, C.J., 2019. Highly heterogeneous depleted mantle recorded in the lower oceanic crust. Nat. Geosci. 12, 482-486.
- Lambart, S., Hamilton, S., Lang, O.I., 2022. Compositional variability of San Carlos olivine. Chemical Geology 605 (120968). https://doi.org/10.1016/j. chemgeo.2022.120968.
- Laporte, D., Toplis, M.J., Seyler, M., Devidal, J.L., 2004. A new experimental technique for extracting liquids from peridotite at very low degrees of melting: application to partial melting of depleted peridotite. Contrib. Mineral. Petrol. 146, 463-484.
- Laporte, D., Lambart, S., Schiano, P., Ottolini, L., 2014. Experimental derivation of nepheline syenite and phonolite liquids by partial melting of upper mantle peridotites. Earth Planet. Sci. Lett. 404, 319–331.
- Le Roux, V., Lee, C.T., Turner, S.J., 2010. Zn/Fe systematics in mafic and ultramafic systems: implications for detecting major element heterogeneities in the Earth's mantle. Geochim. Cosmochim. Acta 74, 2779-2796.
- Le Roux, V., Dasgupta, R., Lee, C.T., 2011. Mineralogical heterogeneities in the Earth's mantle: constraints from Mn, Co, Ni and Zn partitioning during partial melting. Earth Planet. Sci. Lett. 307, 395-408.
- Le Roux, V., Dasgupta, R., Lee, C.T.A., 2015. Recommended mineral-melt partition coefficients for FRTEs (Cu), Ga, and Ge during mantle melting. Am. Mineral. 100, 2533\_2544
- Lee, C.T.A., Leeman, W.P., Canil, D., Li, Z.X.A., 2005. Similar V/Sc systematics in MORB and arc basalts: implications for the oxygen fugacities of their mantle source regions. J. Petrol. 46 (11), 2313-2336.
- Liang, Y., Sun, C., Yao, L., 2013. A REE-in-two-pyroxene thermometer for mafic and ultramafic rocks. Geochim. Cosmochim. Acta 102, 246-260.
- Liu, X., Xiong, X., Audétat, A., Li, Y., Song, M., Li, L., Ding, X., 2014. Partitioning of copper between olivine, orthopyroxene, clinopyroxene, spinel, garnet and silicate melts at upper mantle conditions. Geochim. Cosmochim. Acta 125, 1-22.
- Mallik, A., Lambart, S., Chin, E.J., 2021. Tracking the evolution of magmas from heterogeneous mantle sources to eruption. In: Konter, J., Ballmer, M., Cottaar, S., Marquardt, H. (Eds.), Mantle Convection and Surface Expressions. Geophysical Monograph, 263, pp. 153-176. https://doi.org/10.1002/9781119528609.ch6.
- Mallmann, G., O'Neill, H.S.C., 2009. The crystal/melt partitioning of V during mantle melting as a function of oxygen fugacity compared with some other elements (Al, P, Ca, Sc, Ti, Cr, Fe, Ga, Y, Zr and Nb). J. Petrol. 50 (9), 1765-1794.
- Mallmann, G., Burnham, A.D., Fonseca, R.O., 2021. Mineral-melt partitioning of redoxsensitive elements. Magma Redox Geochem. 345-367.
- Matjuschkin, V., Brey, G.P., Höfer, H.E., Woodland, A.B., 2014. The influence of Fe3+ on garnet-orthopyroxene and garnet-olivine geothermometers. Contrib. Mineral. Petrol. 167 (2), 1–10.
- Matzen, A.K., Baker, M.B., Beckett, J.R., Stolper, E.M., 2013. The temperature and pressure dependence of nickel partitioning between olivine and silicate melt. J. Petrol. 54, 2521-2545.
- McDonough, W.F., Sun, S.S., 1995. The composition of the Earth. Chem. Geol. 120 (3-4), 223-253.
- Mourey, A.J., Shea, T., Lynn, K.J., Lerner, A.H., Lambart, S., Costa, F., Oalmann, J., Lee, R.L., Gansecki, C., 2022. Trace elements in olivine fingerprint the source of 2018 magmas and shed light on explosive-effusive eruption cycles at Kīlauea Volcano. Earth Planet. Sci. Lett. 595, 117769.

- Neave, D.A., Shorttle, O., Oeser, M., Weyer, S., Kobayashi, K., 2018. Mantle-derived trace element variability in olivines and their melt inclusions. Earth Planet. Sci. Lett. 483, 90-104
- Nimis, P., Grütter, H., 2010. Internally consistent geothermometers for garnet peridotites and pyroxenites. Contrib. Mineral. Petrol. 159, 411-427.
- O'Reilly, S.Y., Griffin, W.L., 1995. Trace-element partitioning between garnet and clinopyroxene in mantle-derived pyroxenites and eclogites: PTX controls. Chem. Geol. 121 (1-4), 105-130.
- Pattison, D.R.M., Newton, R.C., 1989. Reversed experimental calibration of the garnetclinopyroxene Fe-Mg exchange thermometer. Contrib. Mineral. Petrol. 101, 87–103.
- Pearson, D.G., Davies, G.R., Nixon, P.H., 1993. Geochemical constraints on the petrogenesis of diamond facies pyroxenites from the Beni Bousera peridotite massif, North Morocco. J. Petrol. 34, 125-172.
- Pertermann, M., Hirschmann, M.M., 2003a. Anhydrous partial melting experiments on MORB-like eclogite: phase relations, phase compositions and mineral-melt partitioning of major elements at 2–3 GPa. J. Petrol. 44, 2173–2201.
- Pertermann, M., Hirschmann, M.M., 2003b. Partial melting experiments on a MORB-like pyroxenite between 2 and 3 GPa: constraints on the presence of pyroxenite in basalt source regions from solidus location and melting rate. J. Geophys. Res. Solid Earth 108 (B2).
- Pertermann, M., Hirschmann, M.M., Hametner, K., Günther, D., Schmidt, M.W., 2004. Experimental determination of trace element partitioning between garnet and silicarich liquid during anhydrous partial melting of MORB-like eclogite. Geochem. Geophys. Geosyst. 5.
- Pickering-Witter, J., Johnston, A.D., 2000. The effects of variable bulk composition on the melting systematics of fertile peridotitic assemblages. Contrib. Mineral. Petrol. 140 (2), 190–211.
- Rasmussen, M.B., Halldórsson, S.A., Gibson, S.A., Guðfinnsson, G.H., 2020. Olivine chemistry reveals compositional source heterogeneities within a tilted mantle plume beneath Iceland. Earth Planet. Sci. Lett. 531, 116008.
- Rautela, O., Chapman, A.D., Shields, J.E., Ducea, M.N., Lee, C.T., Jiang, H., Saleeby, J., 2020. In search for the missing arc root of the Southern California Batholith: PTt evolution of upper mantle xenoliths of the Colorado Plateau Transition Zone. Earth Planet. Sci. Lett. 547, 116447.
- Ravna, K., 2000. The garnet-clinopyroxene Fe2+-Mg geothermometer: an updated calibration. J. Metamorph. Geol. 18, 211–219.
- Regula, A., 2020. Experimentally Generated Partition Coefficients for the First-Row Transition Elements during Eclogite Partial Melting at Three Gigapascals. PhD diss. University of Minnesota, 2020.
- Ross, C.R., Keppler, H., Canil, D., O'Neill, H.S.C., 1996, Structure and crystal-field spectra of  $Co_3Al_2$  (SiO<sub>4</sub>)<sub>3</sub> and (Mg, Ni)<sub>3</sub>Al<sub>2</sub>(SiO<sub>4</sub>)<sub>3</sub> garnet. Am. Mineral. 81 (1–2), 61-66.
- Schwab, B.E., Johnston, A.D., 2001. Melting systematics of modally variable, compositionally intermediate peridotites and the effects of mineral fertility. J. Petrol. 42 (10), 1789-1811.
- Seitz, H.M., Altherr, R., Ludwig, T., 1999. Partitioning of transition elements between orthopyroxene and clinopyroxene in peridotitic and websteritic xenoliths: new empirical geothermometers, Geochim, Cosmochim, Acta 63 (23-24), 3967-3982.
- Shorttle, O., Maclennan, J., 2011. Compositional trends of Icelandic basalts: implications for short-length scale lithological heterogeneity in mantle plumes. Geochem. Geophys. Geosyst. 12.
- Shorttle, O., Maclennan, J., Lambart, S., 2014. Quantifying lithological variability in the mantle. Earth Planet. Sci. Lett. 395, 24-40.
- Sigmarsson, O., Steinthórsson, S., 2007. Origin of Icelandic basalts: a review of their petrology and geochemistry. J. Geodyn. 43 (1), 87-100.
- Smith, D., Arculus, R.J., Manchester, J.E., Tyner, G.N., 1994. Garnet-pyroxeneamphibole xenoliths from Chino Valley, Arizona, and implications for continental lithosphere below the Moho. J. Geophys. Res. Solid Earth 99, 683–696. Snetsinger, K.G., Bunch, T.E., Keil, K., 1968. Electron microprobe analysis of vanadium
- in the presence of titanium. Am. Min. 53 (9-10), 1770-1773.
- Sobolev, A.V., Hofmann, A.W., Sobolev, S.V., Nikogosian, I.K., 2005. An olivine-free mantle source of Hawaiian shield basalts. Nature 434 (7033), 590-597.
- Sobolev, A.V., Hofmann, A.W., Kuzmin, D.V., Yaxley, G.M., Arndt, N.T., Chung, S.L., Danyushevsky, L.V., Elliott, T., Frey, F.A., Garcia, M.O., Gurenko, A.A., Kamenetsky, V.S., Kerr, A.C., Krivolutskaya, N.A., Matvienkov, V.V., Nikogosian, I. K., Rocholl, A., Sigurdsson, I.A., Sushchevskaya, N.M., Teklay, M., 2007. The amount of recycled crust in sources of mantle-derived melts. Science 316, 412-417.
- Stosch, H.G., 1981. Sc, Cr, Co and Ni partitioning between minerals from spinel peridotite xenoliths. Contrib. Mineral. Petrol. 78, 166-174.
- Sun, C., Lissenberg, C.J., 2018. Formation of fast-spreading lower oceanic crust as revealed by a new Mg-REE coupled geospeedometer. Earth Planet. Sci. Lett. 487, 165-178
- Usui, T., Righter, K., Shearer, C.K., Jones, J.H., 2022. Effect of sulfur on siderophile element partitioning between olivine and a primary melt from the martian mantle. Am. Min. 107 (3), 357-368.
- Veter, M., Foley, S.F., Mertz-Kraus, R., Groschopf, N., 2017. Trace elements in olivine of ultramafic lamprophyres controlled by phlogopite-rich mineral assemblages in the mantle source. Lithos 292, 81-95.
- Vidito, C., Herzberg, C., Gazel, E., Geist, D., Harpp, K., 2013. Lithological structure of the Galápagos Plume. Geochem. Geophys. Geosyst. 14 (10), 4214-4240.
- Walter, M.J., 1998. Melting of garnet peridotite and the origin of komatiite and depleted lithosphere. J. Petrol. 39, 29-60.
- Wang, X.J., Chen, L.H., Hanyu, T., Shi, J.H., Zhong, Y., Kawabata, H., Miyazaki, T. Hirahara, Y., Takahashi, T., Senda, R., Chang, Q., Vaglarov, B.S., Kimura, J.I., 2021. Linking chemical heterogeneity to lithological heterogeneity of the Samoan mantle

- plume with Fe-Sr-Nd-Pb isotopes. J. Geophys. Res. Solid Earth 126 (12) e2021JB022887.
- Wasylenki, L.E., Baker, M.B., Kent, A.J., Stolper, E.M., 2003. Near-solidus melting of the shallow upper mantle: partial melting experiments on depleted peridotite. J. Petrol. 44 (7), 1163–1191.
- Witt-Eickschen, G., O'Neill, H.S.C., 2005. The effect of temperature on the equilibrium distribution of trace elements between clinopyroxene, orthopyroxene, olivine and spinel in upper mantle peridotite. Chem. Geol. 221 (1–2), 65–101.
- Witt-Eickschen, G., Palme, H., O'neill, H.S.C., Allen, C.M., 2009. The geochemistry of the volatile trace elements As, Cd, Ga, In and Sn in the Earth's mantle: new evidence from in situ analyses of mantle xenoliths. Geochim. Cosmochim. Acta 73 (6), 1755–1778.
- Workman, R.K., Hart, S.R., Jackson, M., Regelous, M., Farley, K.A., Blusztajn, J., Kurz, M., Staudigel, H., 2004. Recycled metasomatized lithosphere as the origin of the Enriched Mantle II (EM2) end-member: evidence from the Samoan Volcanic Chain. Geochem. Geophys. Geosyst. 5 (4).
- Xu, R., Liu, Y., Lambart, S., Hoernle, K., Zhu, Y., Zou, Z., Zhang, J., Wang, Z., Li, M., Moynier, F., Zong, K., Chen, H., Hu, Z., 2022. Decoupled Zn-Sr-Nd isotopic composition of continental intraplate basalts caused by two-stage melting process. Geochim. Cosmochim. Acta 326, 234–252.
- Yang, S., Humayun, M., Salters, V.J., 2020. Elemental constraints on the amount of recycled crust in the generation of mid-oceanic ridge basalts (MORBs). Sci. Adv. 6.